The Plant Cell, Vol. 30: 563–581, March 2018, www.plantcell.org © 2018 ASPB.

TEOSINTE BRANCHED1 Regulates Inflorescence Architecture and Development in Bread Wheat (*Triticum aestivum*)[OPEN]

Laura E. Dixon,[a,1] Julian R. Greenwood,[b,1] Stefano Bencivenga,[a] Peng Zhang,[c] James Cockram,[d] Gregory Mellers,[d] Kerrie Ramm,[b] Colin Cavanagh,[b,2] Steve M. Swain,[b] and Scott A. Boden[a,3]

[a] Department of Crop Genetics, John Innes Centre, Norwich NR4 7UH, United Kingdom
[b] CSIRO Agriculture and Food, Canberra, ACT 2601, Australia
[c] Plant Breeding Institute, School of Life and Environmental Sciences, University of Sydney, Cobbitty, NSW 2570, Australia
[d] John Bingham Laboratory, National Institute of Agricultural Botany, Cambridge CB3 0LE, United Kingdom

ORCID IDs: 0000-0002-8234-3407 (L.E.D.); 0000-0002-4191-1068 (P.Z.); 0000-0001-7295-3407 (G.M.); 0000-0003-1390-5952 (K.R.); 0000-0001-5297-4067 (S.A.B.)

The flowers of major cereals are arranged on reproductive branches known as spikelets, which group together to form an inflorescence. Diversity for inflorescence architecture has been exploited during domestication to increase crop yields, and genetic variation for this trait has potential to further boost grain production. Multiple genes that regulate inflorescence architecture have been identified by studying alleles that modify gene activity or dosage; however, little is known in wheat. Here, we show *TEOSINTE BRANCHED1* (*TB1*) regulates inflorescence architecture in bread wheat (*Triticum aestivum*) by investigating lines that display a form of inflorescence branching known as "paired spikelets." We show that TB1 interacts with FLOWERING LOCUS T1 and that increased dosage of *TB1* alters inflorescence architecture and growth rate in a process that includes reduced expression of meristem identity genes, with allelic diversity for *TB1* found to associate genetically with paired spikelet development in modern cultivars. We propose *TB1* coordinates formation of axillary spikelets during the vegetative to floral transition and that alleles known to modify dosage or function of *TB1* could help increase wheat yields.

INTRODUCTION

A grass inflorescence is a group of seed-producing flowers that are arranged on specialized branches, known as spikelets. A plant's reproductive success is strongly influenced by the number and arrangement of spikelets and flowers that form on an inflorescence, known as inflorescence architecture, as this determines the maximum number of sites available for seed production. Consequently, diversity for inflorescence architecture has been important during the domestication of crop plants, as modifications that increase flower number have helped improve yields (Meyer and Purugganan, 2013; Zhang and Yuan, 2014). This diversity is often influenced genetically by alleles that alter the dosage of genes involved in spikelet and floret development (Doebley et al., 1997; Simons et al., 2006; Miura et al., 2010; Jiao et al., 2010; Yoshida et al., 2013; Houston et al., 2013; Zhu et al., 2013; Park et al., 2014; Greenwood et al., 2017; Debernardi et al., 2017; Soyk et al., 2017). An increased understanding of the genes that regulate spikelet and floret development, and selection of alleles that alter the activity of these genes, can therefore be used as a tool to increase crop yields (Miura et al., 2010; Jiao et al., 2010; Yoshida et al., 2013; Park et al., 2014; Wang et al., 2015; Soyk et al., 2017).

Bread wheat (*Triticum aestivum*) produces an inflorescence with a unique architecture among crops, forming single spikelets on opposite sides of a central rachis in an alternating phyllotaxy and a terminal spikelet at the apex, with each spikelet producing multiple florets. The number of spikelets that form on an inflorescence and the number of fertile florets in each spikelet are two major determinants of yield and are influenced by the rate of inflorescence development (Rawson, 1970; Miralles et al., 2000; Slafer, 2003; González et al., 2011). Despite the importance of these traits for grain production and the potential for improvements to contribute to yield increases required to feed the world's growing population, very little is known about how they are regulated genetically (Reynolds et al., 2009; González-Navarro et al., 2015). Recent studies have investigated wheat lines with modified inflorescence architectures to identify genes that contribute to spikelet development, including our analysis of "paired spikelets" (Dobrovolskaya et al., 2015; Boden et al., 2015; Poursarebani et al., 2015). Paired spikelets are a form of supernumerary spikelets characterized by the formation of two precisely positioned spikelets at a given rachis node rather than the typical single spikelet (Boden et al., 2015; Sharman, 1944), which are distinct from other supernumerary spikelet structures including long lateral branches that form at the base of an inflorescence, and multirowed spikelets characterized by the formation of multiple spikelets at individual nodes (Dobrovolskaya et al., 2015; Poursarebani et al., 2015; Sharman, 1967). Paired spikelet development is regulated by multiple genes, with quantitative trait

[1] These authors contributed equally to this work.
[2] Current address: Bayer CropScience SA-NV, J.E. Mommaertslaan 14, 1831 Diegem, Machelen, Belgium.
[3] Address correspondence to scott.boden@jic.ac.uk.
The author responsible for distribution of materials integral to the findings presented in this article in accordance with the policy described in the Instructions for Authors (www.plantcell.org) is: Scott A. Boden (scott.boden@jic.ac.uk).
[OPEN] Articles can be viewed without a subscription.
www.plantcell.org/cgi/doi/10.1105/tpc.17.00961

IN A NUTSHELL

Background: Grass inflorescences are composed of many seed-producing flowers (or florets) that are arranged on branches called spikelets. The number and arrangement of spikelets that form on an inflorescence, and the rate of inflorescence development, contribute significantly to the grain yield of major cereals (including wheat, rice, and maize). However, while bread wheat (*Triticum aestivum*) provides 20% of the world's calories and protein, very little is known about the genes that control its inflorescence development. To identify genes that regulate spikelet development in wheat, we investigated a trait known as paired spikelets, which are characterized by the formation of two spikelets at a position where usually only one spikelet forms.

Question: The aim of our study was to investigate genes that regulate inflorescence development in bread wheat and to increase our understanding of the molecular processes involved in generating the different morphologies of cereal grass inflorescences.

Findings: We demonstrated that *TEOSINTE BRANCHED1* (*TB1*) is a gene that regulates inflorescence architecture and development of bread wheat in a dosage-dependent manner. We show that increased levels of TB1 promote development of paired spikelets in a process that involves an interaction with FLOWERING LOCUS T (FT) protein (a key regulator of flowering) and reduced expression of meristem identity genes during early inflorescence development. We have also found that variant alleles of *TB1* contribute to diversity for inflorescence architecture in cultivated wheat.

Next steps: An important step now will be to determine the ideal combination of *TB1* and *FT* alleles (alternative forms of these genes) that could be used to optimize inflorescence development and grain production in bread wheat and to investigate the contribution of variant *TB1* alleles to other agronomically important traits such as tiller number, plant height, and floret fertility.

locus (QTL) analysis of a four parent multiparent advanced generation intercross (MAGIC) population detecting 18 QTLs that contribute to this trait (Boden et al., 2015). One of the QTLs detected in this study was underpinned by *Photoperiod-1* (*Ppd-1*), a pseudo-response regulator gene that controls photoperiod response pathways in wheat (Beales et al., 2007). We found that *Ppd-1* regulates inflorescence architecture by controlling the expression of the central regulator of flowering, *FLOWERING LOCUS T1* (*FT1*), which modulates the strength of the flowering signal perceived in the developing inflorescence. Alleles of *Ppd-1* and *FT1* that produce a weak flowering signal facilitated paired spikelet production through reduced expression of genes that regulate spikelet development, relative to *Ppd-1* and *FT1* alleles that produce a strong flowering signal and suppress paired spikelet formation (Boden et al., 2015).

In this study, we investigated a pair of near-isogenic lines (NILs) developed from the MAGIC population to demonstrate that an ortholog of the maize (*Zea mays*) domestication gene, *TEOSINTE BRANCHED1* (*TB1*), regulates wheat inflorescence architecture in a dosage-dependent manner. We show that TB1 protein interacts with FT1 and that increased dosage of *TB1* promotes paired spikelet production and delays inflorescence growth by reducing expression of meristem identity genes during early developmental stages. We also identify variant alleles for *TB1* on the B and D wheat genomes and show that these alleles are at least partially responsible for diversity of inflorescence architecture in modern wheat cultivars.

RESULTS

The Bread Wheat *hb* Line Displays Inflorescence and Plant Architecture Phenotypes

To identify genes that regulate inflorescence architecture in wheat, we investigated a pair of near-isogenic lines (NILs) derived from a single line of a four-parent MAGIC population for spring wheat (Huang et al., 2012). This line (MAGIC line 0053) was chosen because individuals within field plots displayed either wild-type inflorescences or inflorescences with multiple paired spikelets, suggesting that alleles for one or more gene(s) regulating spikelet architecture were segregating within this line. Seeds were independently selected from plants with wild-type and paired spikelet-producing inflorescences over multiple generations (Supplemental Figure 1) to produce true-breeding lines that formed either wild-type inflorescences or highly branched inflorescences with multiple paired spikelets (Figure 1A), which will henceforth be referred to as *highly-branched* (*hb*). In *hb* plants, 43.3% $\pm$ 3.8% of nodes on the inflorescence (aka rachis nodes) produced paired spikelets, with 28.7% $\pm$ 3.9% of all nodes containing fertile secondary spikelets (Figure 1B). Consistent with our previous analysis of this trait (Boden et al. 2015), paired spikelets were found most frequently at central nodes of the inflorescence, and secondary spikelets formed immediately adjacent to and directly below the primary spikelet during early developmental stages (Supplemental Figure 2).

As paired spikelet development is facilitated by genetic and environmental conditions that delay flowering and is associated with an increase in the number of positions (nodes) available for spikelet production, we tested if flowering time and rachis node numbers were affected in *hb* plants, relative to the wild type (Sharman, 1944; Boden et al., 2015). Under long-day photoperiods (16 h light/8 h dark), we observed no difference in the number of days until inflorescence emergence or the number of rachis nodes between the two genotypes, confirming that paired spikelet production is independent of flowering time in these lines (Figures 1C and 1D). However, we did notice a slight increase in the total leaf number of *hb* plants, relative to the wild type, suggesting that inflorescence development is delayed in *hb* plants (Figure 1E).

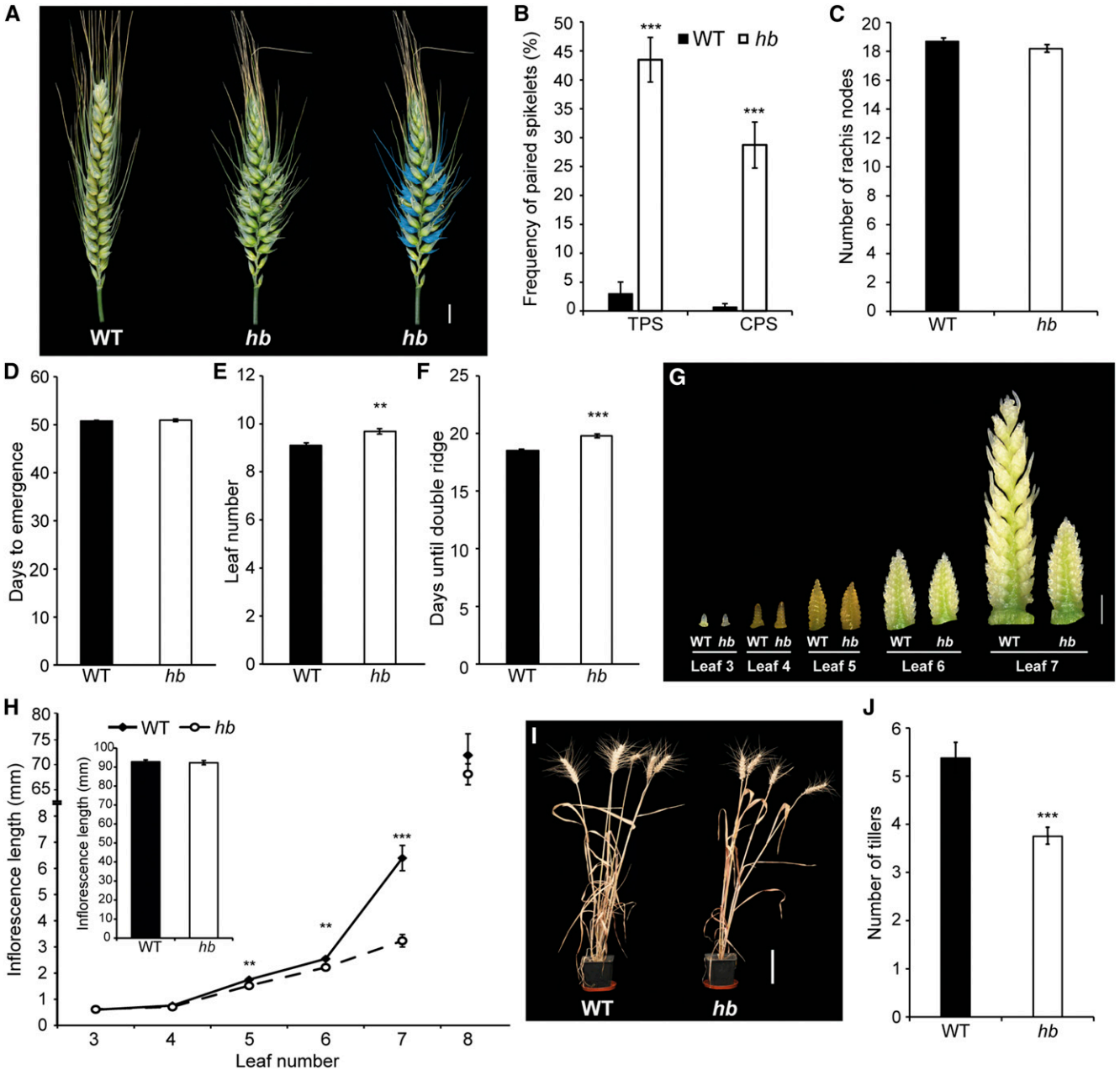

Figure 1. Inflorescence Architecture and Development and Tiller Number Are Modified in *hb* Plants.

(A) Wild-type (WT) and *hb* inflorescences (an image with secondary spikelets highlighted in blue is shown at the right). Bar = 1 cm.
(B) and **(C)** Frequency of total paired spikelets (TPS) and complete fertile paired spikelets (CPS) **(B)** and rachis node numbers of wild type (black) and *hb* (white) inflorescences **(C)**.
(D) and **(E)** Flowering time of wild-type and *hb* plants, measured by days to head emergence **(D)** and total leaf number **(E)**.
(F) Days until double ridge (since germination) for the wild type and *hb*.
(G) and **(H)** Inflorescence development phenotypes of wild-type (solid line) and *hb* (dashed line) plants, measured at intervals defined by leaf emergence. Inset in **(H)** is mature inflorescence length for the wild type and *hb.* Bar = 1 mm.
(I) and **(J)** Tiller numbers of wild-type and *hb* plants. Bar = 10 cm.
Data are mean ± SE. $n = 8$ plants for **(B)** and **(C)**, $n = 10$ for **(D)** to **(F)** and **(J)**, $n = 4$ for **(H)**, and $n = 10$ for **(H)** inset. All images are representatives of individuals used for quantification. **$P < 0.01$ and ***$P < 0.001$, compared with wild-type values.

To investigate this further, we analyzed the time required for shoot apical meristems (SAMs) of wild-type and *hb* lines to reach the double-ridge stage, which is the stage immediately after the vegetative-to-reproductive transition of the SAM occurs. We found that SAMs of wild-type plants reached the double-ridge stage earlier than *hb* plants, which explains the slight increase in leaf number of *hb* plants, relative to the wild type (Figures 1E and 1F).

Further investigation of inflorescence development and growth in *hb* plants, relative to wild-type plants, at intervals defined by leaf emergence from leaf 3 (L3) until leaf 8 (L8) revealed that there were also significant delays of inflorescence growth in *hb* plants at stages L5 and L6, which is when the terminal spikelet forms and spikelet primordia begin developing florets (Figures 1G and 1H). Growth of *hb* inflorescences was delayed dramatically at the L7 stage, relative to the wild type; the delay was allayed by L8, when no difference in inflorescence length was detected between the two genotypes (Figure 1H; Supplemental Figure 3). There was also no significant difference in the length of mature inflorescences between the two genotypes (inset of Figure 1H) nor was there a significant difference in leaf emergence or leaf elongation, suggesting that the inflorescence development and growth phenotypes are not the consequence of a delayed plastochron (Supplemental Figure 4). In addition to the inflorescence phenotypes, we found that *hb* plants produced fewer tillers than wild-type plants (Figures 1I and 1J). Dissection of leaf sheaths surrounding immature tillers showed that the *hb* plants produced tiller buds at each vegetative node that were smaller than those produced in wild-type plants (Supplemental Figure 5), suggesting that the reduced tiller numbers in the *hb* plants were due to suppressed outgrowth of the tiller buds rather than failure to develop tillers. Taken together, these results suggest that there is a pleiotropic effect on growth of lateral organs from the main shoot in *hb* plants, relative to the wild type.

Chromosome 4D Is Duplicated in *hb* Lines

To identify the genetic factor(s) contributing to the inflorescence and plant architecture phenotypes of the *hb* NIL, we initially performed genotype analysis using the 90,000 single nucleotide polymorphism wheat array (Wang et al., 2014), which suggested there was a partial or complete duplication of chromosome 4D (data not shown). To investigate this further, we performed cytogenetic analysis of chromosomes from wild-type and *hb* plants, which showed that the *hb* line is tetrasomic for chromosome 4D, suggesting that increased dosage of chromosome 4D facilitates paired spikelet formation (Figures 2A and 2B). To test if regulation of paired spikelets by chromosome 4D dosage is a dominant or semidominant trait, we crossed the *hb* line to two spring wheat cultivars that do not produce paired spikelets: Sunstate and Pastor. Phenotype analysis showed that the first filial generation (F1) of offspring for both crosses produced paired spikelets (Supplemental Figure 6). As paired spikelet development was reduced in the F1 plants of the *hb* crosses, relative to the tetrasomic *hb* line, we conclude that this is a semidominant trait (Figure 1B; Supplemental Figure 6).

TB-D1 Expression Is Increased in Inflorescences and Tillers of *hb* Lines

Our previous analysis of QTLs that contribute to paired spikelet development within the four parent MAGIC population detected a QTL with a significant additive genetic effect on the short arm of chromosome 4D (4DS), which was detected using a marker positioned within the major Green Revolution gene *Rht-D1* (*Reduced height-D1*; *Rht-2*) (Boden et al., 2015). Dominant dwarfing alleles for *Rht-1* and *Rht-2* (*Rht-B1b* and *Rht-D1b*, respectively) restrict plant growth and impede inflorescence development by reducing the plant's sensitivity to the growth-promoting hormone gibberellin (Pearce et al., 2011; Hedden, 2003; Boden et al., 2014). Both the wild-type and *hb* lines contain the *Rht-B1b* (dwarfing) and *Rht-D1a* (wild-type) alleles, and we hypothesized that reduced sensitivity to gibberellin via increased dosage of *Rht-D1a* may facilitate paired spikelet development by restricting growth of spikelet meristems and the developing inflorescence. To test this hypothesis, we examined inflorescence architecture in a pair of NILs that contained either the wild-type *Rht-D1a* allele or the dwarfing *Rht-D1b* and in *Rht-D1c* (*Rht10*) lines that contain multiple copies of *Rht-D1b* (Pearce et al., 2011), relative to its NIL that contains a single copy. We did not detect paired spikelets in either of these genotypes, suggesting that increased dosage of *Rht-D1* is not responsible for the modified inflorescence architecture of the *hb* line (Supplemental Figure 7).

Through our analysis of *Rht-D1* and the surrounding genetic region underlying the QTL on 4D, we noticed that a wheat ortholog of an important maize domestication gene, *TB1*, is closely linked to *Rht-D1* (Figure 2C). *TB1* encodes a class II TCP (TEOSINTE BRANCHED1, CYCLOIDEA, PCF1) transcription factor, which is a member of a plant-specific family of transcription factors that bind to promoter regions of genes known to regulate developmental processes including branching, floral symmetry, leaf development, and germination (Doebley et al., 1997; Luo et al., 1996; Kosugi and Ohashi, 1997; Tatematsu et al., 2008). *TB1* orthologs regulate tiller number and influence inflorescence architecture traits in maize, rice (*Oryza sativa*), and barley (*Hordeum vulgare*) (Doebley et al., 1995, 1997; Takeda et al., 2003; Studer et al., 2011; Ramsay et al., 2011), with the dominant *Tb1* allele of domesticated maize restricting growth of lateral branches via increased gene expression, relative to the *tb1* allele of the wild progenitor, teosinte (*Zea mays* ssp *parviglumis*) (Doebley et al. 1997); we therefore hypothesized that increased dosage of the wheat *TB1* ortholog from the D genome (*TB-D1*) may be responsible for the paired spikelet and tiller phenotypes of *hb* plants.

Using digital droplet PCR (ddPCR), we confirmed that *hb* plants contain a haploid complement of two copies for *TB-D1*, and wild-type plants contain one copy (Figure 2D). We then compared expression levels for *TB1* from the A (*TB-A1*), B (*TB-B1*), and D genomes in wild-type and *hb* plants at defined stages of inflorescence development and in vegetative tissues that included tiller buds, emerging tillers, leaves, roots, and germinating seedlings. We observed that *TB-B1* and *TB-D1* are expressed predominantly in developing inflorescences and tillers, relative to leaves, roots, and seedlings, and that *TB-A1* expression is significantly lower than that of *TB-B1* and *TB-D1* (Figures 2E and 2F; $P < 0.0001$). Our analysis showed that *TB-B1* and *TB-D1* were

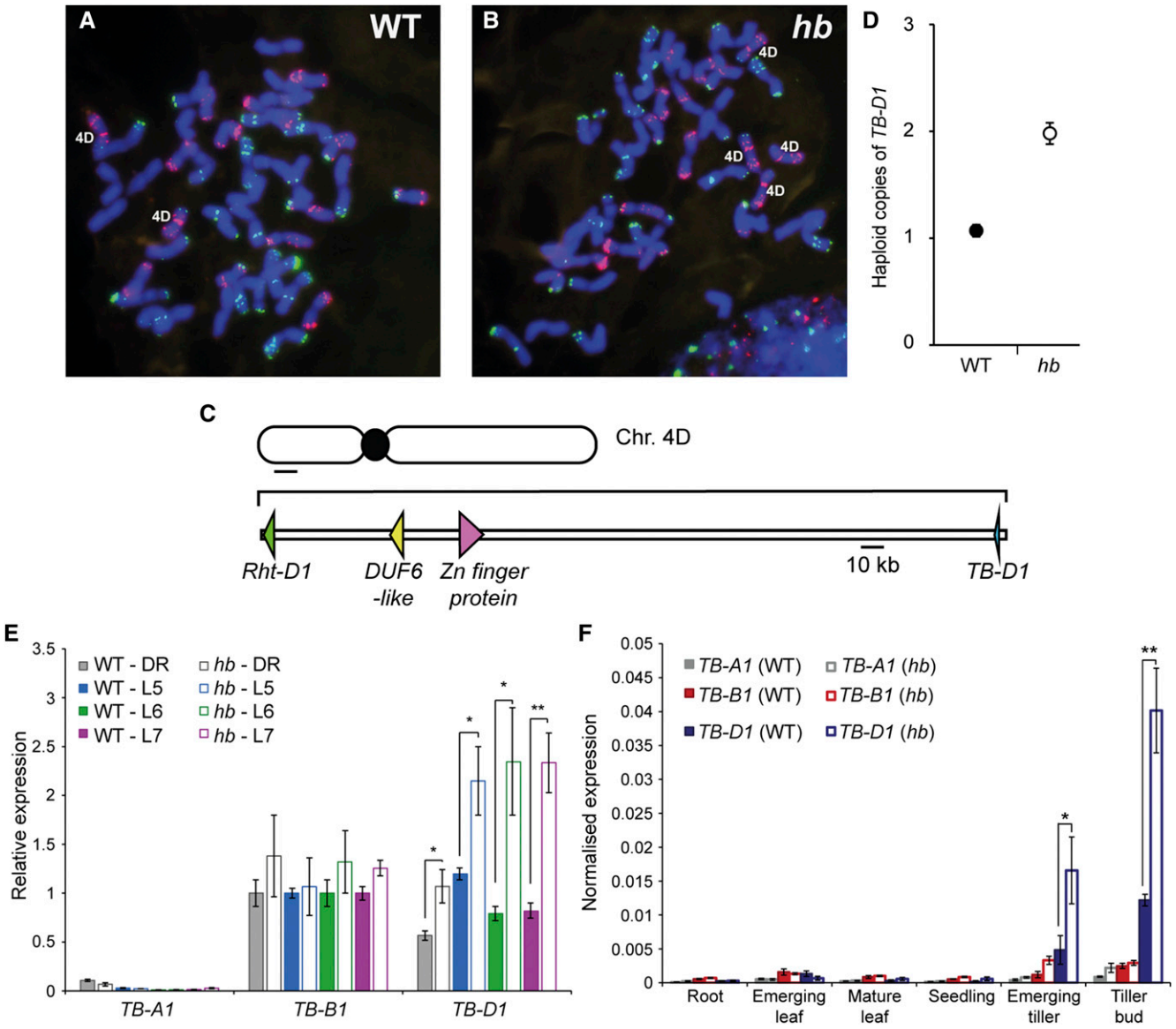

Figure 2. Genetic Characterization and Expression Analysis Reveal Increased Dosage of *TB-D1* in *hb* NILs.

(A) and **(B)** FISH analysis of wild-type **(A)** and *hb* **(B)** lines; copies of chromosome 4D are labeled.

(C) Schematic diagram of chromosome 4DS region in proximity to *Rht-D1*. Gene identities: *DUF6-like* gene, TRIAE_CS42_4DS_TGACv1_362748_AA1181880; *Zn-finger protein*, TRIAE_CS42_4DS_TGACv1_363130_AA1183390.

(D) ddPCR analysis of haploid gene copy number for *TB-D1* in wild-type (black) and *hb* (white) lines.

(E) Relative expression of *TB-A1*, *TB-B1*, and *TB-D1* in developing inflorescences of wild-type (solid bars) and *hb* (white bars) plants, at double ridge (DR; gray), leaf 5 (L5; blue), leaf 6 (L6; green), and leaf 7 (L7; magenta) developmental stages. Expression is relative to *TB-B1* in the wild type.

(F) Expression analysis of *TB-A1* (gray), *TB-B1* (red), and *TB-D1* (purple) in vegetative tissues of wild-type (solid bars) and *hb* (white bars) plants. Data of ddPCR and expression analyses are mean ± SE of three to four biological replicates. *P < 0.05 and **P < 0.01, compared with wild-type values.

expressed comparably in developing inflorescences and emerging tillers, and transcript levels for both genes were 4- to 10-fold higher in tiller buds (Supplemental Figure 8). We found that *TB-D1* transcript levels were significantly higher in developing inflorescences of *hb* plants, relative to the wild type, at the double-ridge stage of development that is pivotal for paired spikelet formation (Boden et al., 2015) and during the L5–L7 developmental stages when inflorescence growth is delayed in *hb* plants (Figures 1G and 2E). We also detected a significant increase in *TB-D1* transcripts in tiller buds and emerging tillers of *hb* plants, relative to the wild type, while no significant difference in *TB-D1* transcript levels were detected between the two genotypes in roots, leaves, or germinating seedlings (Figure 2F). These results demonstrate that *TB-D1* transcript levels are

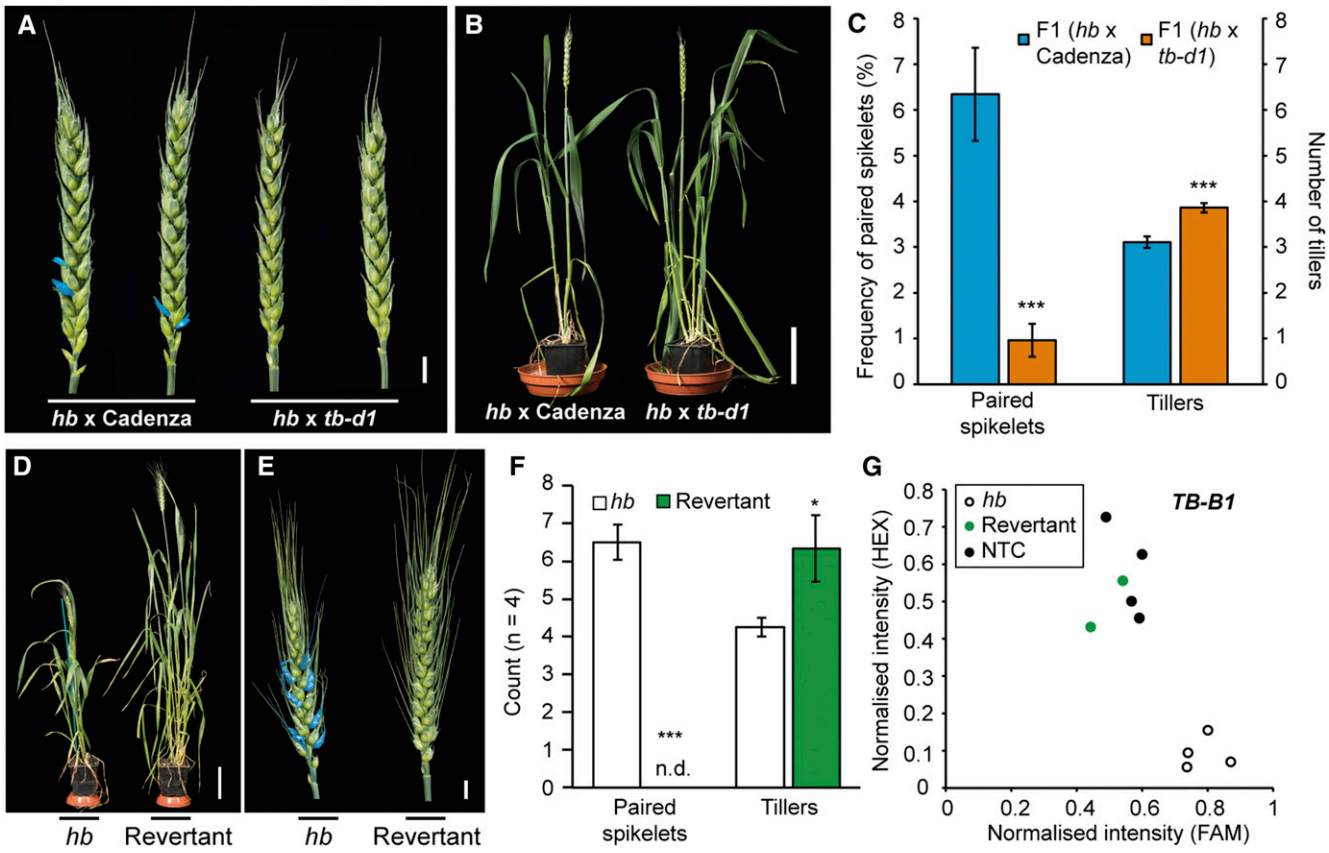

Figure 3. Increased Dosage of *TB1* Regulates Paired Spikelet and Tiller Phenotypes in *hb* Plants.

(A) to **(C)** Inflorescence (**[A]** and **[C]**) and plant (**[B]** and **[C]**) architecture phenotypes of F1 offspring plants from crosses between *hb* and cv Cadenza (WT), *hb*, and the *tb-d1* mutant line (*Cadenza1721*), with quantification **(C)** of frequency of nodes with secondary spikelets per inflorescence (given as total paired spikelets) and tillers per plant.

(D) to **(F)** Plant **(D)** and inflorescence **(E)** architecture phenotypes of *hb* and revertant lines, with quantification **(F)** of paired spikelets per inflorescence and tillers per plant. Secondary spikelets are highlighted in blue. n.d., not detected.

(G) KASP marker analysis of *TB-B1* in *hb* (white) and revertant (green) lines, along with no template control (NTC; black).

Bars = 10 cm in **(B)** and **(D)** and 1 cm in **(A)** and **(E)**. All images are representatives of individuals used for quantification. In **(C)**, data are mean ± SE of 29 F1 plants for *hb* x Cadenza and 50 plants for *hb* x *tb-d1*. *P < 0.05 and ***P < 0.001, compared with values for the F1 (*hb* x Cadenza) in **(C)** and to *hb* in **(F)**.

significantly higher in tissues of the *hb* plants that display architecture phenotypes, relative to wild-type plants, which was not observed for most other genes that are in proximity to *TB-D1* on chromosome 4D (Supplemental Figure 9). These results are therefore supportive of increased *TB-D1* expression promoting paired spikelet development and suppressing tiller outgrowth.

TB-D1 Regulates Inflorescence and Plant Architecture in a Dosage-Dependent Manner

To confirm genetically that *TB-D1* is the gene responsible for the inflorescence and plant architecture phenotypes observed in *hb* plants, we crossed the *hb* line to a wheat TILLING mutant of cultivar Cadenza (Krasileva et al., 2017), line *Cadenza1721*, which contains a premature stop codon mutation (C>T, 49 bp of coding sequence) in *TB-D1* and is henceforth referred to as *tb-d1*. As the crosses to Sunstate and Pastor showed that increased dosage of chromosome 4D is semidominant for paired spikelet production (Supplemental Figure 6), we hypothesized that F1 plants trisomic for chromosome 4D that contain two functional copies and one nonfunctional copy of *TB-D1* (*hb* x *tb-d1*) would not produce paired spikelets and would produce more tillers, relative to F1 plants trisomic for chromosome 4D that contain three functional copies of *TB-D1* (*hb* x Cadenza). Analysis of 29 F1 plants from the *hb* x Cadenza cross supported the results from the *hb* x Sunstate and *hb* x Pastor crosses, with F1 plants found to develop paired spikelets (6.34% ± 1.02% of nodes) (Figures 3A and 3C). Conversely, F1 plants of the *hb* x *tb-d1* cross did not produce paired spikelets (45 plants) or formed rudimentary secondary spikelets at a very low frequency (one per inflorescence; five plants) (Figures 3A and 3C). F1 plants of the *hb* x *tb-d1* cross also produced more tillers (3.86 ± 0.1) than the *hb* x Cadenza F1 plants (3.1 ± 0.125; P < 0.001) (Figures 3B and 3C). Based on these results, we conclude that *TB-D1* is likely to be the gene responsible for the paired spikelet and tiller number phenotypes caused by increased dosage of chromosome 4D in the *hb* line.

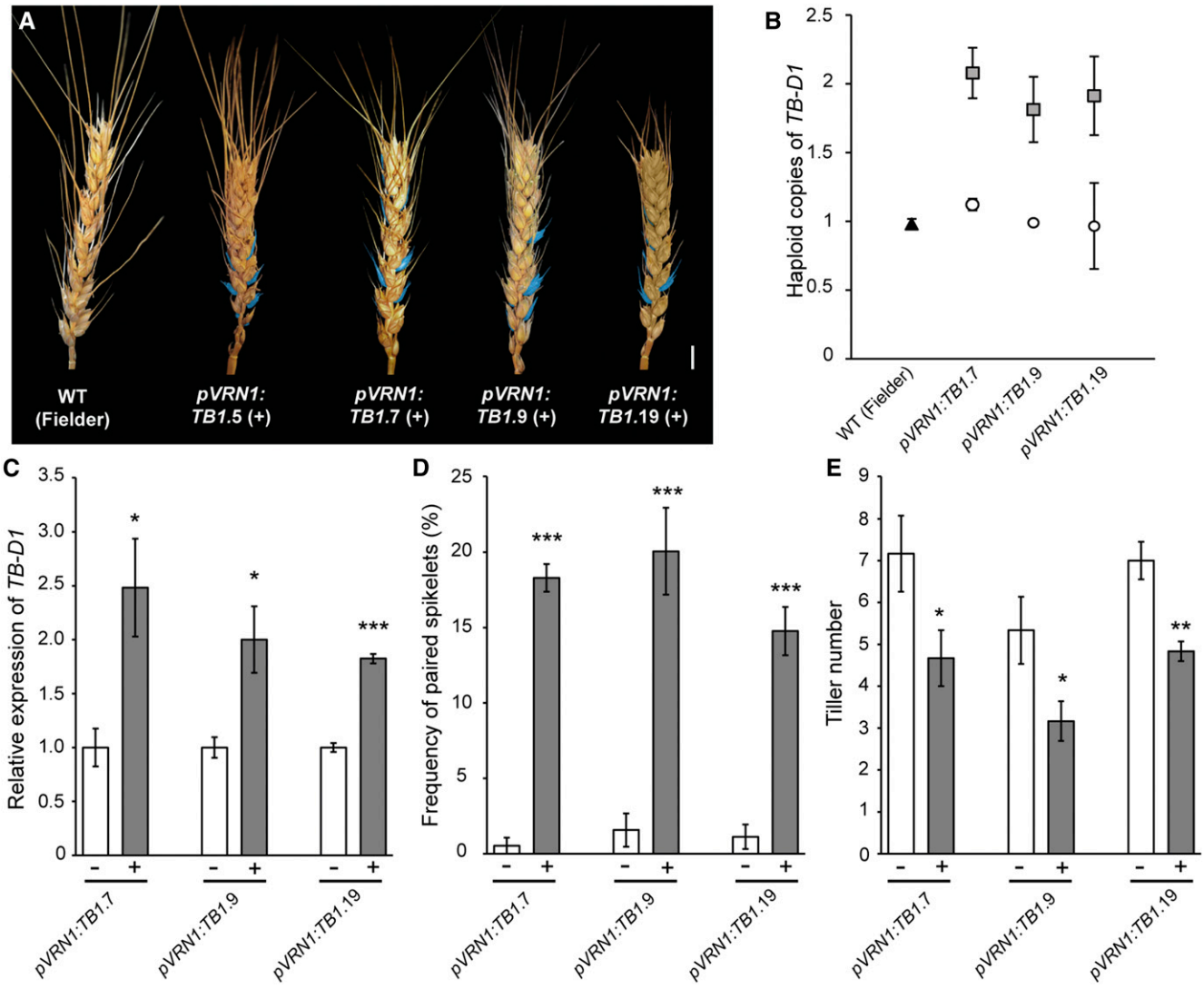

Figure 4. Increased Dosage of *TB-D1* Promotes Paired Spikelet Development and Reduces Tiller Number in Transgenic Lines.

(A) Inflorescences of *pVRN1:TB1* transgenic plants (T1 generation), and the wild-type untransformed control (Fielder). Secondary spikelets are highlighted in blue. Bar = 1 cm.

(B) *TB-D1* haploid gene copy number for *pVRN1:TB1* transgenic plants (gray) and control (white, null transgenic; black, Fielder) lines.

(C) *TB-D1* expression in developing inflorescences of *pVRN1:TB1* transgenic lines (gray), relative to null siblings (white).

(D) and **(E)** Frequency of paired spikelets (**[D]**; given as total paired spikelets) and tiller number phenotypes **(E)** for *pVRN1:TB1* transgenic lines (gray), relative to null siblings (white).

For **(C)**, data are mean ± SE of 4 biological replicates; for **(D)** and **(E)**, data are mean ± SE of 3 to 5 biological replicates. *$P < 0.05$, **$P < 0.01$, and ***$P < 0.001$, compared with values for null siblings.

This conclusion was further supported by analysis of plants from a revertant line that derived spontaneously from an individual *hb* plant, which no longer formed paired spikelets, produced more tillers, and were significantly taller than *hb* plants (Figures 3D to 3F; Supplemental Table 1). We hypothesized that the increased height of these plants was caused by loss of the dwarfing *Rht-B1b* allele and that the absence of paired spikelets and increased tiller numbers occurred through loss of the closely linked *TB-B1*, possibly through loss of chromosome 4B. Marker analysis confirmed that *TB-B1* and *Rht-B1b* were indeed absent in the revertant lines (Figure 3G; Supplemental Figure 10). Taken together with the results from F1 plants of the *hb* x *tb-d1* cross and the expression analysis, we conclude that increased dosage of *TB1*, with contributions from both the wheat D and B genomes, promotes paired spikelet development and reduces outgrowth of tillers in *hb* plants.

To further confirm genetically that increased dosage of *TB-D1* promotes paired spikelet development in wheat, we generated

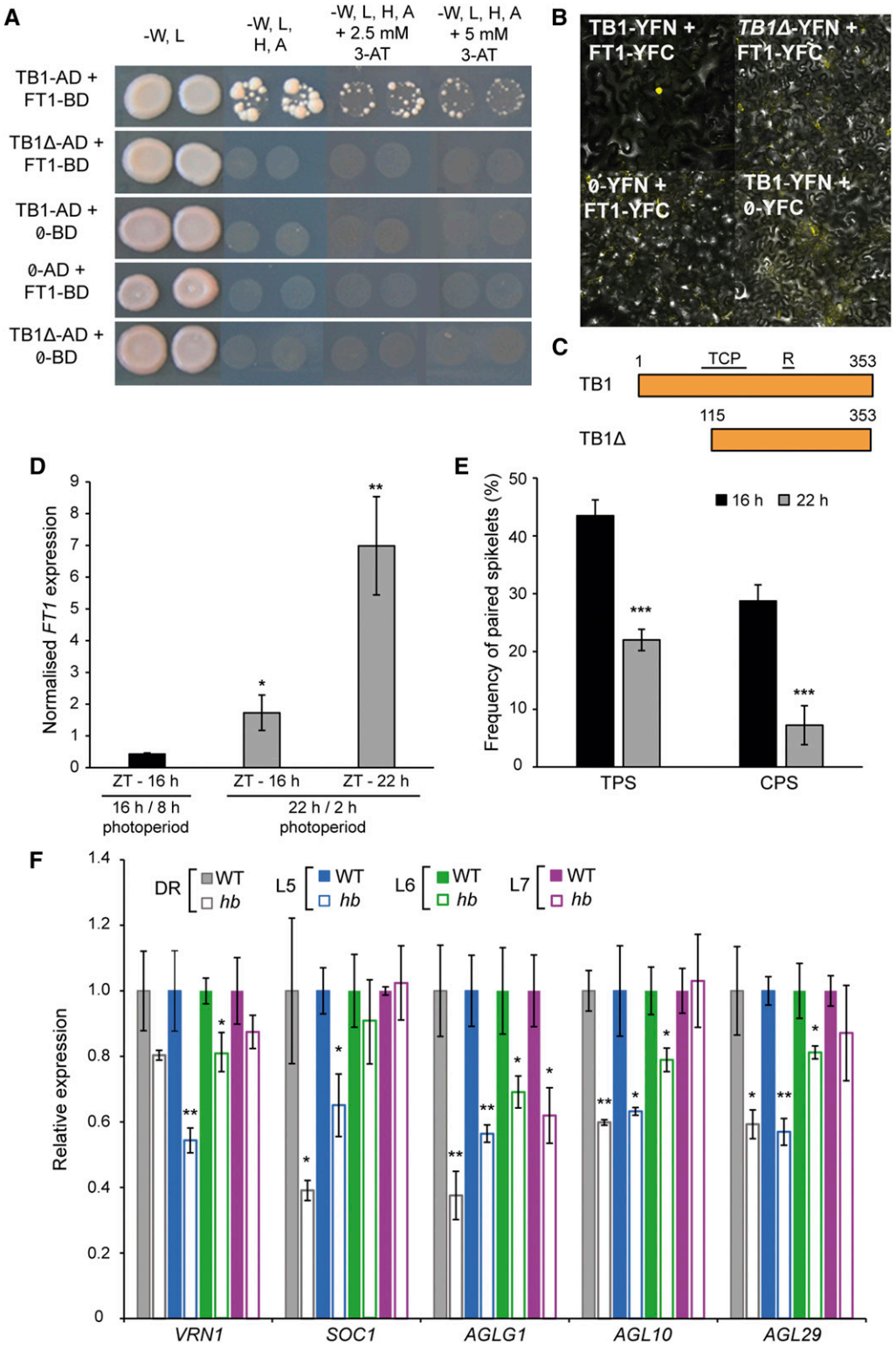

Figure 5. TB1 Interacts with FT1 and Modulates Expression of Meristem Identity Genes.

(A) Y2H assay between TB1 and FT1, including control reactions with truncated TB-D1 (TB1Δ) and empty vectors (Ø), grown on varying selective media.
(B) BiFC assay for TB1 and FT1, and control reactions including truncated TB-D1 (TB1Δ) and empty vectors (Ø).

transgenic lines that expressed *TB-D1* using the well-characterized promoter of *VERNALIZATION1* (*VRN1*) (Alonso-Peral et al., 2011) in the genetic background of Fielder, which forms paired spikelets at a very low frequency. *VRN1* encodes a MADS box transcription factor that is expressed robustly in the developing inflorescence during the vegetative to reproductive transition, including the double-ridge stage when paired spikelets form (Yan et al., 2003; Alonso-Peral et al., 2011; Boden et al., 2015). We also confirmed that *VRN1* is expressed in tiller buds and emerging tillers of wild-type plants (Supplemental Figure 11). The *VRN1* promoter was used because initial attempts to overexpress *TB-D1* using the *Ubiquitin* and *Actin1* promoters failed to produce transgenic seedlings, and sequence for the *TB-D1* promoter was not available. This experiment therefore increased the number of genomic copies for *TB-D1* and promoted expression of the additional copies of *TB-D1* within the inflorescence at stages pivotal for paired spikelet development. From this experiment, we identified 14 independent *pVRN1:TB-D1* transgenic lines that formed paired spikelet-producing inflorescences (Figure 4; Supplemental Figure 12 and Supplemental Table 2). Genotype analysis of T1 transgenic lines identified lines that contained 1.5 or 2 haploid copies of *TB-D1*, while null transgenic plants and control Fielder plants contained 1 haploid copy of *TB-D1* (Figure 4B; Supplemental Table 2). We selected three independent *pVRN:TB1* lines to perform molecular and phenotypic analysis of T2 generation plants: *pVRN:TB1.7*, *9*, and *19* (Figures 4C to 4E). RT-qPCR analysis showed that *TB-D1* transcript levels were significantly higher in the developing inflorescences of each positive transgenic line, relative to their respective null transgenic siblings (Figure 4C). Phenotype analysis showed that inflorescences of the *pVRN:TB1* transgenic lines formed secondary spikelets at 15 to 20% of the rachis nodes and produced fewer tillers than the null transgenic lines, which did not produce secondary spikelets (Figures 4D and 4E). These results therefore confirm our hypothesis that increased dosage of *TB1* promotes paired spikelet development and reduces tiller outgrowth in wheat.

TB1 Interacts with FT1 and Expression of Meristem Identity Genes Is Reduced in Lines with Increased Dosage of *TB-D1*

To identify how increased *TB1* dosage may promote paired spikelet development, we surveyed the literature for molecular interactions that involve *TB1* orthologs and associate with genetic pathways known to influence inflorescence architecture. In *Arabidopsis thaliana*, rice, and wheat, the central integrator of flowering FT interacts with FLOWERING LOCUS D (FD; or FDL in wheat) and 14-3-3 proteins to form a floral activating complex, which induces expression of floral meristem identity genes (Abe et al., 2005; Wigge et al., 2005; Taoka et al., 2011; Li et al., 2015). It has also been shown that the Arabidopsis homolog of *TB1*, *BRANCHED1* (*BRC1*) (Aguilar-Martínez et al., 2007), negatively regulates the vegetative-to-reproductive transition of axillary branches by interacting with FT and suppressing its ability to promote expression of floral meristem identity genes (Niwa et al., 2013). As we have shown previously that deletion of *FT-B1* promotes paired spikelet development (Boden et al., 2015), we hypothesized that TB-D1 interacts with FT1 and that increased dosage of *TB-D1* facilitates paired spikelet development by reducing the availability of FT1 to promote expression of spikelet meristem identity genes within the developing inflorescence.

To test this hypothesis, we performed yeast two-hybrid (Y2H) and bimolecular fluorescence complementation (BiFC) analysis to determine if TB-D1 and FT1 proteins interact. Both the Y2H and BiFC analyses demonstrated that TB-D1 interacts directly with FT1, while no interaction was detected in control experiments, which included a truncated version of TB-D1 (TB1Δ) that lacks the first 115 amino acids of TB1, a region demonstrated previously to be essential for the interaction between BRC1 and FT from Arabidopsis (Figures 5A to 5C; Supplemental Figure 13) (Niwa et al., 2013). To test this interaction further and determine if the effect of increased TB-D1 levels could be suppressed by enhanced *FT1* activity, we grew *hb* plants under extended long-day (LD) conditions (22-h/2-h photoperiod) and standard LD conditions (16 h/8 h). Under the extended LD conditions, *FT1* transcript levels were significantly higher at dusk (Zeitgeber time [ZT] 22 h) and at the time point that would correspond to dusk in the standard LD photoperiod (ZT 16 h), relative to the levels at dusk under the standard LD conditions (ZT 16 h; Figure 5D).

We also found that paired spikelet development is significantly suppressed under the extended LD photoperiod, with reduced production of total paired spikelets and secondary spikelets with fertile florets, relative to plants grown under standard LD (Figure 5E). We then tested if increased dosage of *TB-D1* affects expression of genes that regulate spikelet development by analyzing transcript levels of meristem identity genes from developing inflorescences of wild-type and *hb* plants (Figure 5F). These genes included *VRN1*, *SOC1*, *AGAMOUS-LIKE GENE1*, *AGAMOUS-LIKE10* (*AGL10*), and *AGL29*, whose expression was found previously to be reduced in inflorescences of paired spikelet producing lines, including a mutant containing a deletion of *FT-B1* (Boden et al., 2015). We found that transcript levels for all meristem identity genes were significantly reduced during early developmental stages in inflorescences of *hb* plants, relative to those of wild-type plants (except for *VRN1* at the DR stage), which included stages pivotal for paired spikelet development (Figure 5F). This result was supported by analysis showing that transcript levels for meristem identity genes were

Figure 5. (continued).

(C) Schematic of full-length TB1 and truncated TB1 (TB1Δ) proteins used for Y2H and BiFC assays; TCP and R refer to domains of TB1 protein, and numbers indicate amino acid positions.

(D) and **(E)** Expression analysis of *FT1* at dusk **(D)** and frequency of total paired spikelets (TPS) and complete fertile paired spikelets (CPS) in *hb* plants under standard LD photoperiods (black) and extended LD photoperiods (gray) **(E)**.

(F) Expression of meristem identity genes in developing inflorescences of *hb* (white bars), relative to the wild type (solid bars), at double ridge (DR; gray), leaf 5 (L5; blue), leaf 6 (L6; green), and leaf 7 (L7; magenta) developmental stages. Data are mean ± SE; $n = 4$ biological replicates for **(D)** and **(F)** and $n = 10$ biological replicates for **(E)**. *$P < 0.05$, **$P < 0.01$, and ***$P < 0.001$, compared with standard LD values (**[D]** and **[E]**) and wild-type values **(F)**.

significantly reduced in developing inflorescences of the *pVRN1:TB1* transgenic plants, relative to null transgenic siblings (Supplemental Figure 14). At the leaf 7 developmental stage, transcript levels for *VRN1*, *SOC1*, *AGL10*, and *AGL29* were not significantly different in wild-type and *hb* plants, which is consistent with the observed completion of spikelet and floret development in *hb* inflorescences at the L7 stage in preparation for growth between emergence of L7 and 8 (Figures 1G, 1H, and 5F). We confirmed that the changes in activity of meristem identity genes were not associated with reduced expression of *FT1* in *hb* plants, relative to the wild type (Supplemental Figure 14). Based on these results, we conclude that TB1 interacts with FT1 and that increased dosage of TB1 promotes paired spikelet development and delays inflorescence growth between the L5 and L7 stages by reducing the expression of spikelet meristem identity genes.

Allelic Diversity for *TB1* Regulates Inflorescence Architecture in Modern Wheat Cultivars

As *TB1* contributes to important yield traits including inflorescence architecture and growth in other plants, we hypothesized that there are allelic variants for *TB1* among modern wheat cultivars, which contribute to variation in spikelet development. To test this hypothesis and determine if a *TB1* allele may be responsible for the paired spikelet QTL detected previously on chromosomes 4B and 4D (Boden et al., 2015), we sequenced *TB-B1* and *TB-D1* from the cultivars used to generate the four-parent spring wheat MAGIC population: Baxter, Chara, Westonia, and Yitpi. No sequence polymorphism was detected for *TB-B1* among the four cultivars; however, one polymorphism was detected in the open reading frame of *TB-D1* from Baxter, which is a nonsynonymous mutation (G-328 bp-T; D110Y) at the beginning of the conserved TCP domain (Figure 6A; Supplemental Figures 15 and 16). Interestingly, our previous analysis identified Baxter as the cultivar that contributes a positive genetic effect for the paired spikelet QTL on chromosome 4D that displayed LOD scores of 1.27 to 5.44 across five experiments, which were detected using the marker for *Rht-D1* that is in proximity to *TB-D1* (Boden et al., 2015). Taken together, these results suggest that the Baxter allele for *TB-D1* (referred to as *TB-D1b*) may be responsible for the paired spikelet QTL detected on chromosome 4D.

To gain further evidence of allelic variation for *TB1*, we surveyed 230 modern winter wheat cultivars for paired spikelet development over two growing seasons (Supplemental Figure 17, Supplemental Table 3, and Supplemental Data Set 1). We identified 96 cultivars that produced paired spikelets, including Abbot, Ambrosia, Einstein, Gladiator, and Hyperion, which formed secondary spikelets at 20 to 35% of rachis nodes (Supplemental Figure 17 and Supplemental Table 3). Digital droplet PCR and sequence analysis for *TB-B1* and *TB-D1* on a subset of these cultivars showed that there was no CNV for *TB-B1* or *TB-D1* (Supplemental Figure 18) and no sequence variant alleles for *TB-D1*. However, we did detect an allele for *TB-B1* (referred to as *TB-B1b*) that contained five sequence polymorphisms in complete linkage disequilibrium, including two synonymous mutations (G-198 bp-A, G-912 bp-A) and three nonsynonymous mutations (C-309 bp-G, S103R; A-663 bp-T, K221N; C-812 bp-T, A271V) (Figure 6B; Supplemental Figures 19 and 20). KASP-based marker analysis showed that the *TB-B1b* allele was widely distributed across a geo-referenced panel of 264 European wheat varieties (the GEDIFLUX panel) and was observed most frequently in cultivars of Great Britain, Belgium, and France (Figure 6C; Supplemental Table 4 and Supplemental Data Set 2).

We also found that both the *TB-B1a* (wild type; reference sequence) and *TB-B1b* alleles were present among the founder genotypes used to generate the eight parent UK winter wheat MAGIC population, with Rialto, Robigus, and Soissons containing the *TB-B1a* allele and Alchemy, Brompton, Claire, Hereward, and Xi 19 containing the *TB-B1b* allele (Supplemental Table 4). We hypothesized, therefore, that phenotype and genetic analyses for paired spikelets within this MAGIC population would identify a QTL on chromosome 4B in the region proximal to *TB-B1*. Paired spikelet measurements were recorded for field-grown replicated trials over two successive years (643 lines with two replicates in 2015 and 493 lines with two replicates in 2016), with broad sense heritability estimated at 72.4% and 94.1% for 2015 and 2016, respectively. In both years, genetic mapping identified a highly significant QTL in a region of chromosome 4B that included *TB-B1*, which was bound by markers wsnp_BF482960B_Ta_1_4 (47.64 cM, chr 4B position 28,954,488 bp) and RAC875_c27536_611 (48.65 cM, chr 4B position 32,250,720 bp) and explained 6% and 7.5% of phenotypic variance (R^2) in the 2015 and 2016 trials, respectively (Figure 6D; Supplemental Figure 21 and Supplemental Tables 5 and 6). Alleles donated by Rialto, Robigus, and Soissons were predicted to contribute positively toward the paired spikelet trait, suggesting that the *TB-B1a* allele facilitates paired spikelet development (Supplemental Table 6). This conclusion was supported by *TB-B1*-specific marker analysis of a subset of 212 MAGIC lines that formed either wild-type or paired spikelet-producing inflorescences, which confirmed the *TB-B1a* allele was associated genetically with paired spikelet development (McNemar's Test, $P < 0.05$; Supplemental Table 7). To test if the nonsynonymous mutations of *TB-B1b* alter the function of TB-B1, we performed Y2H analysis to determine if TB-B1a and TB-B1b both interact with FT1. Both proteins interacted with FT1; however, analysis of serial dilutions indicated that the interaction between TB-B1a and FT1 was slightly stronger than the interaction between TB-B1b and FT1 (Figure 6E). These results show that variant *TB1* alleles are present on the B and D genomes of winter and spring wheat, respectively, and that diversity for *TB1* modulates inflorescence architecture in modern wheat cultivars.

DISCUSSION

Inflorescence architecture contributes significantly to seed production in plants and is a major determinant of crop yield. Seed production can be increased by developing inflorescences with more elaborate branching patterns, which can be achieved by breeding with alleles that modify the activity of genes involved in spikelet or floret development (Miura et al., 2010; Jiao et al., 2010; Yoshida et al., 2013; Bommert et al., 2013; Meyer and Purugganan, 2013; Zhu et al., 2013; Park et al., 2014; Poursarebani et al., 2015; Soyk et al., 2017). In this study, we have shown that increased dosage of *TB1* promotes inflorescence branching in the form of

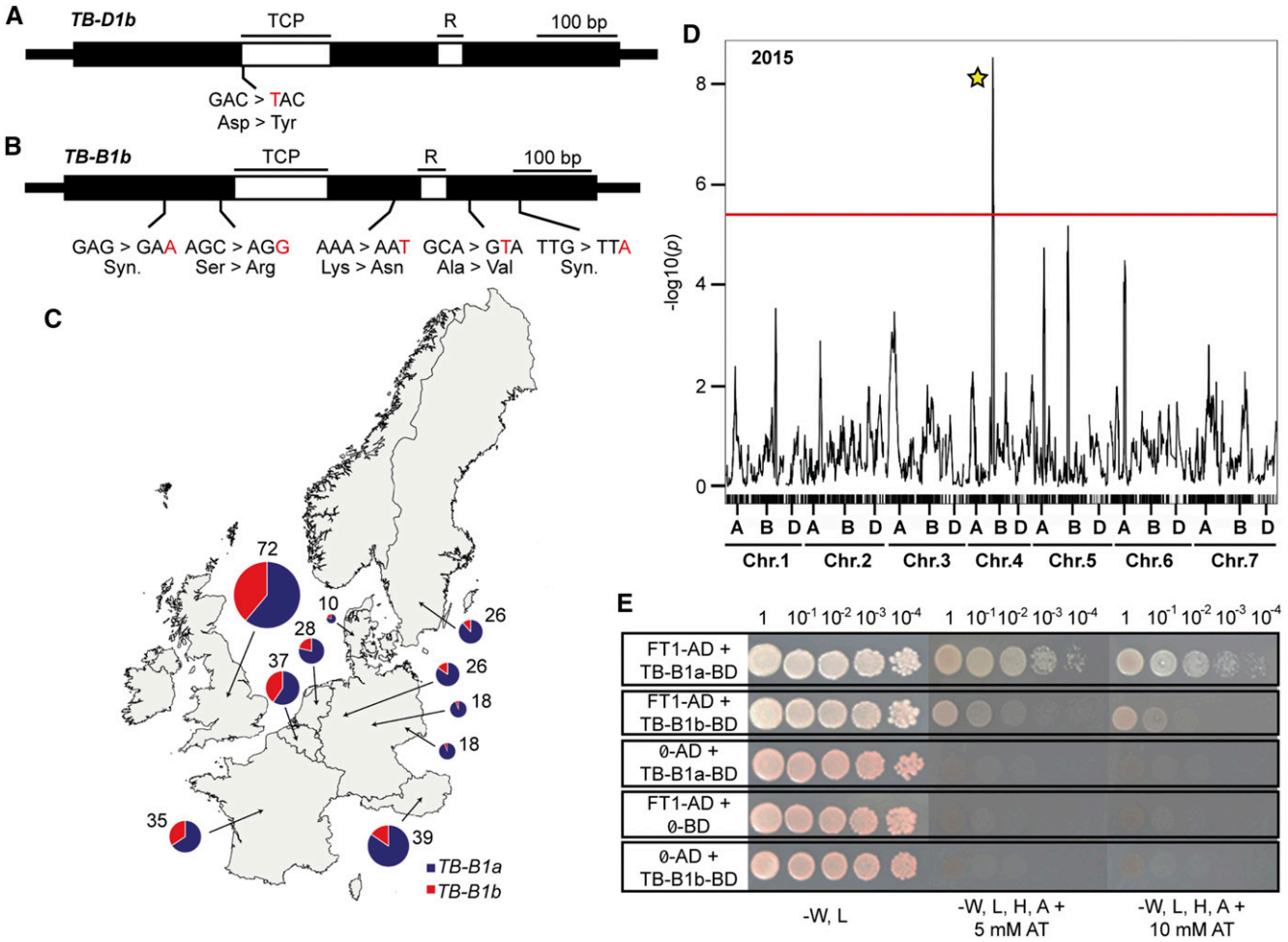

Figure 6. Allelic Variation for *TB-B1* and *TB-D1* Contributes to Inflorescence Architecture Diversity in Spring and Winter Wheat.

(A) and **(B)** Schematic diagrams of variant alleles for *TB-D1* (**[A]**; *TB-D1b*) from spring wheat and *TB-B1* (**[B]**; *TB-B1b*) from winter wheat, with positions of polymorphisms (indicated in red text) and molecular effect indicated (Syn., synonymous). TCP and R refer to genic regions that encode domains of the TB1 protein.

(C) Geographical distribution of *TB-B1a* (purple) and *TB-B1b* (red) alleles in European wheat cultivars of the GEDIFLUX collection.

(D) Genome-wide composite interval mapping scan displaying QTLs that contribute to paired spikelet development from the UK winter wheat MAGIC population from the 2015 trial, including a highly significant QTL on chromosome 4BS (indicated by yellow star). Red line indicates threshold of high significance ($P < 0.01$).

(E) Y2H assay between TB-B1 alleles (TB-B1a and TB-B1b) and FT1, including control reactions with empty vectors (Ø), grown on varying selective media. A 10-fold serial dilution was performed for each interaction experiment.

paired spikelets and that allelic diversity for *TB1* is associated with spikelet architecture traits in modern wheat cultivars.

Our analysis of the near-isogenic and transgenic lines, and the F1 plants from the *hb* x *tb-d1* cross, demonstrates that increased dosage of *TB1* promotes paired spikelet development, which is associated with reduced expression of spikelet meristem identity genes. The reduced expression of the meristem identity genes is consistent with our previous analysis of paired spikelet-producing genotypes that have loss-of-function alleles for key flowering genes, *Ppd-D1* and *FT1* (Boden et al., 2015). Based on these results, and protein interaction experiments that show TB1 interacts with FT1, we propose a model for *TB1*-dependent regulation of inflorescence architecture (Figure 7), whereby increased dosage of *TB1* facilitates paired spikelet development by reducing the availability of FT1 to form part of the floral activating complex and promote expression of spikelet meristem identity genes (Taoka et al., 2011; Boden et al., 2015; Li et al., 2015). This effect of increased *TB1* dosage is consistent with studies of the Arabidopsis *TB1* homolog, *BRC1*, which showed BRC1 is a negative regulator of flowering that interacts with FT and restricts the expression of floral meristem identity genes within axillary meristems (Niwa et al., 2013). We propose that this role for *TB1* is conserved in wheat, where it helps regulate the development of axillary spikelet meristems from the inflorescence meristem during the vegetative to floral transition. At standard levels, *TB1* facilitates formation of unbranched primary spikelets along the inflorescence; however,

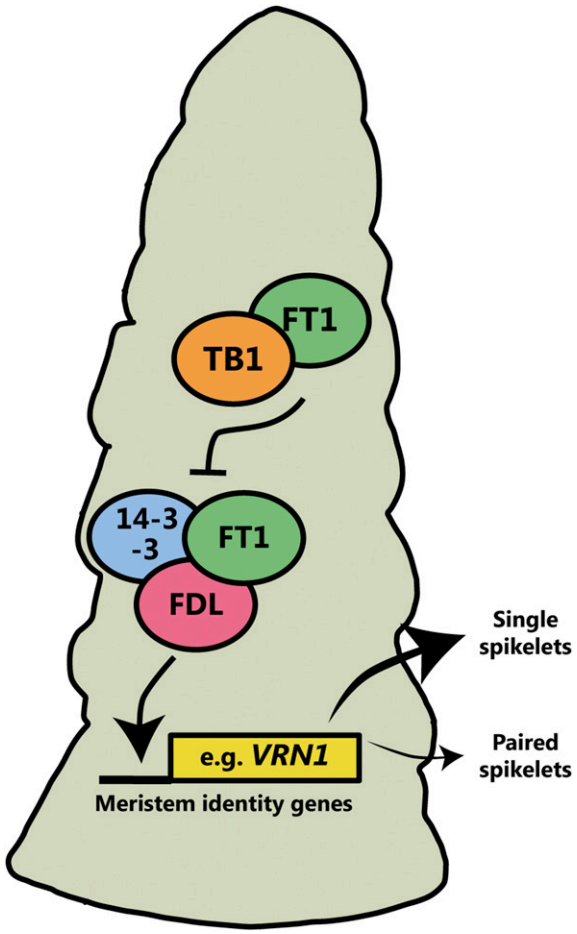

Figure 7. Model Explaining the Effect of Increased Dosage of TB1 on Spikelet Development in Wheat.

Increased levels of TB1 restrict the interaction of FT1 with other members of the floral activating complex (FDL and 14-3-3), which reduces expression of meristem identity genes (e.g., *VRN1*) and facilitates paired spikelet development. At standard levels of TB1, the floral activating complex promotes robust expression of meristem identity genes, and paired spikelet development is suppressed.

when *TB1* levels are increased, the maturation of spikelet meristems is delayed, which results in development of a short branch that is limited to two spikelets (Figure 7). This effect of increased *TB1* levels is consistent with studies performed in rice and tomato (*Solanum lycopersicum*), which have demonstrated that inflorescences with more elaborate branching patterns and increased yields can be developed by reducing the activity of flowering signals and extending the duration of meristem maturation (Park et al., 2012, 2014; Yoshida et al., 2013; Kyozuka et al., 2014; Wang et al., 2015; Lemmon et al., 2016; Soyk et al., 2017). An important area for future analysis will be to use wheat NILs that contain diverse alleles of *TB1* and *FT1* to confirm the TB1:FT1 interaction genetically and to examine the optimum combination of *TB1* and *FT1* alleles for improved inflorescence architecture. These NILs could also be used to investigate possible *TB1*-dependent regulation of inflorescence development and architecture that may occur independently of its interaction with FT1, possibly through regulation of meristem size or meristem dormancy.

Our observation that increased dosage of *TB1* promotes paired spikelet development and reduces tiller numbers in wheat suggests that there is a conserved role for this gene in regulating inflorescence and plant architecture of cereals. In maize, the *Tb1* allele of domesticated cultivars is expressed at a higher level than the *tb1* allele of teosinte, and it suppresses development and growth of axillary branches (Doebley et al., 1997; Hubbard et al., 2002). Consequently, the *Tb1* allele modifies plant architecture by suppressing tiller development to produce a monoculm plant, which is consistent with observations in barley, rice, and wheat that show *TB1* negatively regulates tiller outgrowth (Doebley et al., 1995, 1997; Hubbard et al., 2002; Takeda et al., 2003; Lewis et al., 2008; Ramsay et al., 2011). In regard to inflorescence architecture, the *Tb1* allele contributes to development of maize ears with cupules that contain two spikelets, relative to the less active *tb1* allele of teosinte that is associated with formation of single spikelet cupules (Doebley et al., 1995). Taken together with results shown here, these reports suggest that *TB1* has a conserved role among cereals in regulating the rate at which an axillary meristem completes its development into a spikelet meristem, such that increased dosage of *TB1* delays maturation of the spikelet meristem to promote formation of spikelet pairs rather than single spikelets. This conclusion is supported by a report of wheat plants overexpressing the maize *TB1* gene that produced fewer tillers and formed inflorescences with an increased number and density of rachis nodes and many small spikelets containing incomplete florets, which is consistent with a description of paired spikelets (Lewis et al., 2008). This effect of *TB1* dosage on spikelet architecture may also explain the six-rowed spikelet phenotype of barley lines that contain loss-of-function alleles of the barley *TB1* ortholog, *INTERMEDIUM-C* (*INT-C*/*HvTB1*). Mutant alleles of *HvTB1* facilitate development and outgrowth of fertile lateral spikelets, which are sterile in two-rowed barley that contain the wild-type allele of *HvTB1* (Ramsay et al., 2011). Based on results presented here, the improved fertility of lateral spikelets in barley lines that carry loss-of-function mutant alleles of *HvTB1* may be explained by reduced dormancy of the lateral spikelet primordia and associated with increased expression of meristem identity genes within the lateral spikelets. This hypothesis is supported by results from rice showing that an *OsTB1* allele (*SCM3*) that confers increased *TB1* expression is associated with increased dormancy of axillary meristems to form inflorescences with more primary and secondary panicle branches and that transcript levels of MADS box genes were altered by overexpression of *OsTB1* (Yano et al., 2015). Interestingly, the maize *Tb1* allele has been linked recently to negative transcriptional regulation of MADS box genes in the context of glume development, by suppressing transcription of the Squamosa Promoter Binding protein transcription factor, *teosinte glume architecture1* (Studer et al., 2017). Taken together with the results shown here, these studies suggest that TB1 may act as a transcriptional and posttranslational regulator of genes that control agronomically important traits of inflorescence development, such as MADS box transcription factors. Further investigation of meristem identity gene expression in inflorescences of maize, rice, and barley NILs that contain variant alleles of *Tb1*,

OsTB1, and *INT-C*, respectively, would determine if the *TB1*-dependent mechanism for regulating spikelet architecture is conserved among cereals.

In addition to the inflorescence architecture phenotypes shown here, an important observation from this study is that inflorescence growth was delayed in the *hb* NIL, relative to the wild type, between emergence of leaf 5 and leaf 7. Inflorescence growth rate contributes significantly to floret fertility and is therefore an important component of yield (Miralles et al., 2000; Slafer, 2003; Reynolds et al., 2009). Wheat plants typically produce 10 to 12 floret primordia per spikelet, yet only 2 to 4 of these primordia survive to produce grain; hence, optimization of floret fertility is a key objective for improving wheat yield (Reynolds et al., 2009; González et al., 2011; González-Navarro et al., 2015; Guo and Schnurbusch, 2015). The delayed inflorescence growth of the *hb* NIL, relative to the wild type, suggests that *TB1* dosage influences the rate of inflorescence growth during early developmental stages. It remains to be determined whether this phenotype is directly linked to TB1 function or is a consequence of secondary spikelet development in these lines. However, this result, along with the rapid inflorescence growth that occurs between emergence of leaf 6 and 8, suggests that wheat inflorescences undergo a transition from a phase of axillary organ development to a period of growth in between the terminal spikelet and white anther stages. The timing of this transition correlates developmentally with the stage when the maximum number of viable floret primordia is observed (Guo and Schnurbusch, 2015), suggesting that this may be a point during development when the peak sink potential of the inflorescence is established prior to initiation of inflorescence growth. The conclusion that this growth phenotype is linked to events occurring within the developing inflorescence and is not caused by a delayed plastochron is supported by our analysis showing that leaf emergence and elongation rates were not significantly different between *hb* and wild-type plants. Comparative analysis of gene expression and metabolite levels in inflorescences of wild-type and *hb* NILs during these developmental stages will therefore be useful for identifying molecular pathways that influence the rate of inflorescence growth and floret fertility.

An important outcome of this research is the identification of variant alleles for *TB1* on the B and D wheat genomes that regulate inflorescence architecture in modern wheat cultivars. We identified an alternate allele for *TB-D1* in spring wheat that is a candidate gene for a spikelet architecture QTL detected previously on chromosome 4D (Boden et al., 2015). We also identified a variant allele for *TB-B1* in winter wheat that contains five sequence polymorphisms (*TB-B1b*) and demonstrated that allelic diversity for *TB-B1* contributes to the most significant paired spikelet QTL in the winter wheat MAGIC population. Y2H analysis was performed to investigate the comparative strength of the interaction between FT1 and TB-B1a versus FT1 and TB-B1b, which suggested that TB-B1a interacts more strongly with FT1 than does TB-B1b. Taken together with our genetic analysis of the two *TB-B1* alleles, this result supports our proposed model that increased activity of TB1 promotes paired spikelet development by modulating the function of FT1 (Figure 7). An intriguing outcome from our analysis of multiple wheat cultivars is that many were found to produce paired spikelets, which is surprising given that paired spikelets are undesired within breeding programs because florets of the secondary spikelets often produce small grain that reduces the uniformity of grain size (Crop Committee Handbook, 2013). Taken together with our analysis of *TB1*, this phenomenon may be explained by alleles that promote paired spikelet development also contributing beneficial effects for important yield components of plant development, such as inflorescence growth, floret fertility, or tiller number. Interestingly, we observed that the *TB-B1b* allele appears more frequently in winter wheat cultivars of the UK, France, and Belgium, relative to other regions of Europe; this finding suggests that there may be an adaptive advantage for this allele under certain environmental conditions, which is consistent with the proposed role for *tb1* regulating the plasticity of plant architecture traits of teosinte in response to changes in the local environment (Doebley et al., 1995). Further characterization of these alleles through generation of NILs, or development of CRISPR/Cas9 transgenic lines that target individual polymorphisms within the *TB-B1b* allele, will be important for determining the effect of these mutations on inflorescence and plant architecture. Nonetheless, these results show that variant *TB1* alleles are present on the B and D genomes of winter and spring wheat, respectively, and that diversity for *TB1* modulates inflorescence architecture in modern wheat cultivars.

In summary, we conclude that *TB1* is a key regulator of inflorescence and plant architecture in wheat that interacts with FT1 and regulates axillary spikelet development in a dosage-dependent manner. Our demonstration that increased dosage of *TB1* promotes paired spikelet development is consistent with reports from other crops showing that more elaborate inflorescence branching can be achieved using alleles that modify dosage of gene activity (Doebley et al., 1995; Miura et al., 2010; Jiao et al., 2010; Park et al., 2012, 2014; Yoshida et al., 2013; Bommert et al., 2013; Houston et al., 2013; Zhu et al., 2013; Wang et al., 2015; Soyk et al., 2017). In the case of *TB1*, these results point toward a conserved role for this gene regulating the determinacy and development of axillary spikelet meristems in cereals (Doebley et al., 1995). These results therefore highlight the potential for alleles that modify *TB1* activity to increase the number of flowers available for seed production, which is important given our increasing need to identify genetic traits that will enhance yields of our staple crop plants (Reynolds et al., 2009; Fischer et al., 2014).

METHODS

Plant Materials and Growth Conditions

Hexaploid wheat (*Triticum aestivum*) used in this study included the following genotypes: MAGIC line 0053, from which the NILs termed "wild-type" and "*hb*" were derived (wild type refers to lines of MAGIC line 0053 that form regular inflorescences; Supplemental Figure 1); tall revertant NIL derived from the "*hb*" NIL; transgenic lines expressing *TB-D1* using the *VRN1* promoter generated in the cv Fielder genetic background (see details below); cultivars Sunstate, Pastor, and Cadenza, and the hexaploid wheat TILLING line, *Cadenza1721* (*tb-d1*) (Krasileva et al., 2017); *Rht* NILs (BC_6F_3 NILs in the cv Paragon background, containing either the *Rht-D1b* dwarf allele from cv Alchemy, or the *Rht-D1a* allele from cv Paragon); *Rht-D1c* (aka *Rht10*) (Pearce et al. 2011); and multiple wheat cultivars listed in Supplemental Tables 3 and 4 and Supplemental Data Set 1.

Wild-type *hb* plants, transgenic lines, and the F1 plants of the *hb* crosses to Cadenza, *tb-d1* (*Cadenza1721*), Sunstate, and Pastor that were used for phenotype analysis and gene expression studies were grown in controlled growth chambers under short-day (10 h light/14 h dark) or long-day (16 h light/8 h dark) photoperiods at 300 μmol/m^2/s (using Plantastar 400-W HQI bulbs [Osram] and Maxim 60-W tungsten bulbs), with a day temperature of 20°C and a night temperature of 15°C. Extended photoperiod conditions of 22 h light/2 h dark, as used in speed-breeding (Watson et al., 2018), were used for the *hb* x Cadenza and *hb* x *tb-d1* crosses and to analyze the effect of increased *FT1* activity on paired spikelet development. Winter wheat varieties surveyed for paired spikelet phenotypes were grown at field sites of KWS based in Thriplow, UK (52°06'00.6"N, 0°05'29.1"E) in 1-m^2 plots. Phenotype data for the winter wheat varieties were collected over two growing seasons (2015 and 2016).

The 'NIAB Elite MAGIC' bread wheat population has been previously described (Mackay et al., 2014), and F_8 seed was sourced from NIAB, UK. The paired spikelet phenotype was assessed, following previously published protocols (Boden et al., 2015) but with fertile or infertile classifications for complete PS (resulting in 0–3 scores). PS phenotypes were scored in two field trials; both of which were undertaken at NIAB (52°13'19"N, 0°5′46"E). The first consisted of 643 progeny (2 replicates) and the 8 founders (2 replicates), sown in autumn 2014 and phenotyped at maturity in 2015 (the 2015 trial). The second trial used 493 progeny (2 replicates) and the 8 founders (≥4 replicates), sown in autumn 2015 and phenotyped at maturity in 2016 (the 2016 trial). Each replicate in both trials was sown as two adjacent rows of 1 m each within 1-m^2 plots of six rows total.

Inflorescence Architecture Measurements

Rachis node and paired spikelet measurements were recorded for the inflorescences of the main stem and first tiller. Paired spikelet measurements for each plant have been normalized by calculating the frequency of rachis nodes that contain paired spikelets, represented as a percentage. Data shown for wild-type and *hb* plants is the average ± SE of at least eight plants. Data shown for winter wheat varieties is the average ± SE of four plants, and these varieties were scored in two growing seasons. Data shown for *hb* and tall revertant lines is the average ± SE of at least three plants. Data shown for positive transgenic plants is average ± SD of three to four plants, and for null transgenic plants the data are average ± SD of two to four plants and average ± SD of 10 plants for cv Fielder.

Flowering Time Measurements

Developmental flowering time by total leaf number was determined by counting leaves of the main stem until emergence of the flag leaf. Heading date was measured as the number of days since germination when the inflorescence first emerged from the sheath on the main stem (Zadoks scale, $Z = 47$). Three independent flowering time experiments were performed, with 10 to 20 plants measured in each experiment.

Dissection of Inflorescences and Tillers

Developing inflorescences and immature tillers were isolated with a binocular dissecting microscope and then digitally photographed on a Leica MZ16 Stereo dissecting microscope with a Leica DFC420 color camera. Developing inflorescences were harvested at developmental stages determined by sequential emergence of leaves from germination. Lengths of inflorescences were determined at each developmental stage using Fiji software (Schindelin et al., 2012), with the embedded scale used as a reference. Two independent experiments were performed, with at least four inflorescences measured at each developmental stage. For tiller dissections, six to eight plants were examined of each genotype, with two independent experiments performed.

Paired Spikelet Distribution Analysis

Paired spikelet distribution analysis was performed as described previously (Boden et al., 2015), with 12 inflorescences from six plants (six main stems and six tiller inflorescences) collected and phenotyped from each of the wild-type and *hb* genotypes.

Scanning Electron Microscopy Analysis

Developing inflorescences were dissected from wild-type and *hb* plants, and immediately fixed in 100% ethanol, as described previously (Talbot and White, 2013). Samples were critical point dried using a Leica CPD300 automated critical point drier. Basal spikelets were dissected from dried tissue to expose secondary spikelets of central rachis nodes, and samples were mounted on aluminum stubs with double-sided sticky carbon and coated with gold (~20 nm) using a sputter coater (Agar Scientific). Samples were then examined using a Zeiss Supra 55 scanning electron microscope (Carl Zeiss).

Fluorescence in Situ Hybridization Analysis

Lines were characterized by fluorescence in situ hybridization (FISH) as described previously (Zhang et al., 2004). Plasmid clone pSc119.2 contains highly repetitive sequences from rye (*Secale cereale*; Bedbrook et al., 1980), whereas clone pAs1 contains a repetitive sequence that belongs to the *Afa* family isolated from *Aegilops tauschii* (Rayburn and Gill, 1986). Using two clones simultaneously, all B and D genome chromosomes and chromosomes 1A, 4A, and 5A of hexaploid wheat can be identified (Mukai et al., 1993). One microgram of plasmid DNA of pSc119.2 and pAs1 was labeled with fluorescein-12-dUTP (fluoresces green) and rhodamine-5-dUTP (fluoresces red), respectively, using nick translation in accordance with the manufacturer's protocol (Roche Diagnostics). The hybridization and posthybridization washes were conducted as described previously (Zhang et al., 2004). Chromosomes were counterstained with 4′,6-diamidino-2-phenylindole (Life Technologies) and pseudo-colored blue. Chromosome preparations were analyzed with a Zeiss Axio Imager epifluorescence microscope (Carl Zeiss Microimaging). Images were captured with a Retiga EXi CCD camera (QImaging) operated with Image-Pro Plus 7.0 software (Media Cybernetics) and processed with Photoshop version 8.0 software (Adobe Systems).

Leaf Emergence and Elongation Assays

Wild-type and *hb* plants were grown under LD conditions in a controlled growth chamber. Measurements of leaf emergence were recorded daily from leaf 2 onwards, determined by when the growing tip of the new leaf could be seen emerging from the sheath of the previous leaf. Measurements were recorded for leaf 2 to leaf 8. For leaf elongation assays, length of the emerging leaf blade was recorded daily until growth ceased, which coincided with emergence of the next leaf. Measurements were recorded from leaf 2 to leaf 5. Twelve biological replicates were used for each genotype per experiment, and two independent experiments were performed for each assay.

DNA Extractions and Sequence Analysis

Nucleotide sequences for *TB-A1*, *TB-B1*, and *TB-D1* were obtained by BLAST search from the Ensembl Plants website, using the maize (*Zea mays*) TB1 protein sequence as a query sequence. Genomic DNA extractions were performed as described previously (Paterson et al., 1993). Clones of *TB-B1* and *TB-D1* were amplified using Phusion DNA polymerase (New England Biolabs) and the following oligonucleotides: *TB-B1*, ATGTTTCCTTTCTATGATTCCC, CATCCGGTTCTTTTCCCTAGT, and CGAGGGGAAGAAGCAGGTG, CACAAATAATCCATTGAACAAAGC;

TB-D1, CTCTTCCACCCGCAGACAC, TCAGTAGGGCTGCGAGTTG. DNA fragments were sequenced using the Big-Dye Terminator Sequencing v3.1 Ready Reaction Kit (Perkin-Elmer, Applied BioSystems, Thermo Fischer Scientific) or with Mix2Seq Kit (Eurofins). Multiple nucleotide and protein sequence alignments of *TB-A1*, *TB-B1*, and *TB-D1* were performed using MUSCLE. Pairwise nucleotide and protein sequence alignments of cv Chinese Spring reference sequences for *TB-B1* and *TB-D1* with alleles identified from other wheat varieties were performed using EMBOSS Needle, which were formatted in Microsoft Word. *TB-B1* and *TB-D1* alleles from wheat cultivars that contain sequence polymorphisms relative to the reference sequences from Chinese Spring were named *TB-B1b* and *TB-D1b*, following convention for naming alternate alleles for other wheat genes.

RNA Extraction and Expression Analysis

For experiments with wild-type and *hb* plants, RNA was extracted from tiller, root, young emerging leaf, mature leaf, and seedling tissue using the Spectrum Plant Total RNA Kit (Sigma-Aldrich) and from developing inflorescences using the RNeasy Plant Mini Kit (Qiagen). "Tiller buds" refer to immature tillers that were transparent or light green in color for which no leaf blade had begun to emerge, while "emerging tillers" refers to young tillers where leaf blade tissue was beginning to emerge from the coleoptile-like tissue. RNA was extracted from developing inflorescences at the double-ridge stage and inflorescences harvested at complete emergence of leaf 5, leaf 6, and leaf 7. Analysis of *FT1* expression was performed using RNA extracted from leaves of wild-type and *hb* plants, which were grown under a short-day photoperiod until the leaf 5 stage and then transferred to LD photoperiod for 7 d. For analysis of *FT1* expression under the extended LD photoperiod conditions, *hb* leaf samples were collected at time points corresponding to dusk (i.e., at ZT 16 h for the standard LD photoperiod and ZT 22 h for the extended LD photoperiod), and at 16 h for the extended LD photoperiod to be used as a control time point in reference to dusk collection of the standard LD condition. For experiments with the *pVRN1:TB1* transgenic lines, developing inflorescences were dissected at the spikelet primordium stage, with four inflorescences pooled for each biological replicate sample, and RNA was extracted using the RNeasy Plant Mini Kit (Qiagen). Synthesis of cDNA and RT-qPCR were performed as described previously (Boden et al., 2014). Oligonucleotides for RT-qPCR analysis are provided in Supplemental Table 8. Expression of candidate genes in leaves, roots, tillers, and seedlings was normalized using RNA polymerase 15-kD subunit (*TaRP15*; Shaw et al., 2012) and with Traes_6DS_BE8B5E56D.1 (Borrill et al., 2016) in developing inflorescences. All RT-qPCR data points are the average of at least three biological replicates, with two technical replicates performed in each reaction.

Kompetitive Allele-Specific PCR Analysis

Oligonucleotides for Kompetitive allele-specific PCR (KASP) analysis were designed using Polymarker (http://polymarker.tgac.ac.uk; Ramirez-Gonzalez et al., 2015a) and contained the standard FAM or HEX compatible tails (FAM tail, 5′-GAAGGTGACCAAGTTCATGCT-3′; HEX tail, 5′-GAAGGTCGGAGTCAACGGATT-3′). Oligonucleotide sequences are provided in Supplemental Table 9. The KASP assay was performed as described previously (Ramirez-Gonzalez et al., 2015b), with the following modifications: Assays were set up as 2.4-μL reactions (1.8 μL template [10–20 ng of DNA] dried to assay plate, 1.18 μL of V4 2× Kaspar mix [LGC Group], 1.18 μL deionized water and 0.032 μL primer mix); and the PCR cycling included hotstart at 95°C for 15 min, followed by 10 touchdown cycles (95°C for 20 s; touchdown 65°C, −1°C per cycle, 25 s), followed by 40 cycles of amplification (95°C for 10 s; 57°C for 60 s).

ddPCR Reactions and Data Analysis

ddPCR was performed to determine gene copy numbers for *TB-B1* and *TB-D1*, in reference to *TaCONSTANS2* (*TaCO2*), which has a single copy on each of the three wheat genomes. Oligonucleotide sequences are provided in Supplemental Table 10. The ddPCR reaction mix included 10 μL of 2× QX200 ddPCR EvaGreen Supermix (Bio-Rad), 6 μL of genomic DNA template (2.5 ng/μL; 15 ng), 2 μL of mixed oligonucleotides (2 μM each), and 0.2 μL of *Hind*III-HF (New England Biolabs), in a 20-μL reaction volume. Droplets were generated in eight-well cartridges using the QX200 droplet generator (Bio-Rad). Water-in-oil emulsions were transferred to a 96-well plate and amplified in a C1000 Touch Thermal Cycler (Bio-Rad). Thermal cycling conditions were 7 min at 95°C; 40 cycles of a three-step thermal profile comprising of 30 s at 94°C, 30 s at 60°C, and 1 min at 72°C, with ramp rate 2.0°C/s. After cycling, each sample was incubated at 90°C for 5 min and then cooled to 4°C. Plates were then transferred to the QX200 droplet reader (Bio-Rad). Data acquisition and analysis were performed using QuantaSoft software (Bio-Rad) to quantify numbers of positive droplets containing amplicons and negative droplets without amplicons. Calculations for copy number of *TB-B1* and *TB-D1* were performed in Microsoft Excel. As oligonucleotides for *TaCO2* annealed to sequence and produced amplicons from the A, B, and D genomes, gene copy numbers for *TB-B1* and *TB-D1* were determined by dividing the number of positive droplets for *TB-B1* and *TB-D1* by one-third of the number of positive droplets for *TaCO2*.

Construct Design and Wheat Transformation

The construct used to generate *pVRN1:TB-D1* transgenic plants contained *TB-D1* with the G328T SNP present in cv Baxter, wild-type, and *hb* lines, as well as synonymous mutations (C30G, G309T, and C1023G) that modified restriction sites to facilitate cloning and construct design. *Nco*I and *Not*I sites flanking the start and stop codon positions, respectively, were used to clone *TB-D1* into the *KR PRO 5* plasmid containing the *VRN1* promoter (Alonso-Peral et al., 2011) and the kanamycin resistance gene for selection. The *pVRN1:TB-D1* cassette was cloned into the *vecBarII* construct containing the *Tn7* spectinomycin resistance gene and the *BAR* open reading frame under the regulatory control of the *CaMV 35S* promoter and the *Agrobacterium tumefaciens octopine synthase* terminator sequences.

Transgenic wheat plants were generated by Agrobacterium-mediated transformation of the hexaploid wheat cv Fielder, as described previously (Ishida et al., 2015; Richardson et al., 2014). Genomic DNA extractions were performed as described previously (Paterson et al., 1993), and genotype analysis of T1 transgenic lines was performed as described previously using qRT-PCR (Mieog et al., 2013; Boden et al., 2014) and the $2^{-\Delta\Delta CT}$ method to determine relative copy number for *TB-D1*. Amplicons of *TB-D1* were amplified using oligonucleotides shown in Supplemental Table 10 and were normalized to *Epsilon Cyclase-A1* (oligonucleotides in Supplemental Table 10), which is present once on the "*A*" genome of wheat (Mieog et al., 2013). Normalized levels of *TB-D1* for each transgenic plant were then normalized to those identified for cv Fielder to determine relative copy numbers of *TB-D1* for each transgenic line. Data for RT-qPCR are the average of two technical replicates, with 100 ng of template DNA per reaction. Reactions were performed using the Bio-Rad CFX384 real-time system.

Y2H Analysis

Y2H assays were performed at 28°C in the yeast strain AH109 (Clontech) using the cotransformation technique (Egea-Cortines et al., 1999). Open reading frames of full-length *TB-D1*, *TB-B1a*, *TB-B1b*, and *FT1*, and a truncated version of *TB-D1* (*TB1*Δ) that encodes a protein lacking the first 114 amino acids of the full-length protein. The *TB-D1* allele used here was the allele from Baxter, as this is the allele found in the wild-type and *hb* lines.

These open reading frames were cloned into the Gateway vector GAL4 system (*pGADT7* and *pGBKT7*; Clontech) passing through *pDONR207* (Life Technologies, Thermo Fischer Scientific). Strength of protein interactions was tested on selective yeast synthetic dropout medium (YSD) lacking leucine (L), tryptophan (W), adenine (A), and histidine (H), supplemented with different concentrations of 3-aminotriazole (2.5, 5, and 10 mM). Images were taken 7 d after plating on the selective media.

BiFC Analysis

Open reading frames of full-length *TB-D1* and *FT1*, and truncated *TB1* (*TB1*Δ) in *pDONR207* (Life Technologies) generated for the Y2H assay, were each cloned into *pYFPN43* and *pYFPC43*. *pEAQ-HT* vector (Sainsbury et al., 2009), which expresses the silencing suppressor *p19* of tomato bushy stunt virus, was added to the vector combination. BiFC was performed in *Nicotiana benthamiana* as described previously (Belda-Palazón et al., 2012). Images were taken with a Zeiss LSM780 confocal microscope 72 h after infiltration.

Genetic Analysis of NIAB Elite MAGIC Population

Trial entries were arrayed in an incomplete block design using the software Block Designs U (http://www.expdesigns.co.uk). Paired spikelet phenotype data were analyzed using GenStat (16th edition; VSNi) with a generalized linear mixed model employing a Poisson distribution with a logarithmic link function (Bolker et al., 2009) providing best linear unbiased estimate values. Broad-sense heritability for the replicated trials was calculated as per Equation 1 (Tenesa and Haley, 2013), where σ_g^2 is the genotypic variance and σ^2 is the residual error variance with *r* replicates.

$$H^2 = \frac{\sigma_g^2}{\sigma_g^2 + \frac{\sigma^2}{r}} = \frac{V_g}{V_p} \quad (1)$$

In total, 643 F5 lines from the NIAB Elite MAGIC wheat population (Mackay et al., 2014) were genotyped using a wheat Illumina 90k iSelect array designed by Wang et al. (2014) generating 18,601 polymorphic markers mapped to 7369 unique genetic map locations (Gardner et al., 2016). Using these markers, a high confidence subset of identity by descent (IBD) segments were calculated in a three-point probabilistic manner (Huang and George, 2011) for their parental contributions over the 7369 uniquely mapped markers. Founder probabilities were assigned with a 33% threshold, as identity-by-descent relationships among the founders complicate direct observation of true parental origin. The resulting founder haplotype probabilities were used for composite interval mapping analysis.

QTL analysis was performed using an IBD composite interval mapping (IBD-CIM) method (Milner et al., 2016). IBD-CIM was performed using the mpIM function of the R package mpMap (Huang and George, 2011). Primarily, a linear model was fitted for estimation of the QTL fixed effects for every founder at each hypothetical QTL position (with the founder "Xi19" arbitrarily fixed as the reference haplotype). Simple interval mapping was run and then the inclusion of marker covariates was determined by a forward selection process in an Akaike information criterion-dependent manner, up to a maximum of five covariates. To determine significance thresholds, a null distribution is formed with the same variance as the trial's score data and the significance threshold is then determined empirically. The proportion of phenotypic variance explained by any given QTL, accounting for all other QTL, is the square of the semipartial correlation coefficient (Milner et al., 2016). QTL nomenclature follows recommended rules, as listed in the GrainGenes catalog (https://wheat.pw.usda.gov/ggpages/wgc/98/Intro.htm).

Genetic markers of interest were aligned to the unannotated IWGSC RefSeq v1.0 reference wheat genome sequence (cv Chinese Spring 42; www.wheatgenome.org/) using BLASTn with a maximum E-value threshold of 0.1 (Altschul et al., 1990). Annotation within target regions was undertaken using GMap (Wu and Watanabe, 2005) to map high-confidence TGAC v1 gene models (Clavijo et al., 2017) (cv Chinese Spring 42, Earlham Institute) to IWGSC RefSeq v1.0 using 95% minimum identity and 80% minimum coverage thresholds. The highest scoring BLASTx hit for the resulting gene models in wheat from the SwissProt (The UniProt Consortium, 2017) database were identified with a maximum E-value threshold of one (Supplemental Table 7).

Statistical Analysis

Differences between treatments were tested by two-tailed Student's *t* test. Results in figures are shown as means ± SE, except for Figures 2H and 2I, which show the mean ± SD because some null transgenic lines contained only two individuals. For the *TB-B1*-specific marker analysis of 212 UK winter wheat MAGIC lines, a McNemar's test was performed using 1 degree of freedom.

Accession Numbers

Accession numbers for all genes investigated in this study are provided in Supplemental Tables 8 and 10.

Supplemental Data

Supplemental Figure 1. Schematic outlining pedigree of wild-type and *hb* lines from MAGIC line 0053.

Supplemental Figure 2. Paired spikelet development on *hb* inflorescences.

Supplemental Figure 3. Wild-type and *hb* inflorescences at the leaf 8 developmental stage.

Supplemental Figure 4. Leaf emergence and leaf elongation rates for wild-type and *hb* plants.

Supplemental Figure 5. Immature tillers of wild-type and *hb* plants.

Supplemental Figure 6. Inflorescence architecture phenotypes of F1 offspring from *hb* crosses.

Supplemental Figure 7. Inflorescence architecture phenotypes of *Rht-D1* NILs.

Supplemental Figure 8. Expression analysis of *TB-B1* and *TB-D1* in tillers and developing Inflorescences.

Supplemental Figure 9. Expression analysis of genes from chromosome group 4 that are in proximity to *Rht-1* and *TB1*.

Supplemental Figure 10. KASP marker analysis of *Rht-B1* in *hb* and revertant lines.

Supplemental Figure 11. Expression analysis of *VRN1*.

Supplemental Figure 12. Inflorescence architecture phenotypes of *pVRN1:TB1* transgenic plants.

Supplemental Figure 13. TEOSINTE BRANCHED1 interacts with FLOWERING LOCUS T1.

Supplemental Figure 14. Expression analysis of meristem identity genes and *FLOWERING LOCUS T1*.

Supplemental Figure 15. Alignment of coding nucleotide sequence for *TB-D1a* and *TB-D1b* alleles.

Supplemental Figure 16. Alignment of predicted amino acid sequence for TB-D1a and TB-D1b.

Supplemental Figure 17. Paired spikelet development in modern winter wheat cultivars.

Supplemental Figure 18. Analysis of copy number variation for *TB-D1* and *TB-B1* in winter wheat.

Supplemental Figure 19. Alignment of coding nucleotide sequence for *TB-B1a* and *TB-B1b* alleles.

Supplemental Figure 20. Alignment of amino acid sequence for TB-B1a and TB-B1b.

Supplemental Figure 21. Chromosome-wide CIM scans displaying the 4B QTL that contributes to paired spikelet development in the UK wheat MAGIC population.

Supplemental Table 1. Phenotype information for *hb* revertant lines, relative to *hb*.

Supplemental Table 2. Phenotype information for T1 transgenic *pVRN1:TB1* lines, with controls.

Supplemental Table 3. Proportion of rachis nodes with paired spikelets in subset of modern wheat cultivars.

Supplemental Table 4. *TB-B1* alleles of modern winter wheat cultivars investigated in this study.

Supplemental Table 5. Summary of paired spikelet QTLs identified in the NIAB Elite MAGIC population using IBD-CIM.

Supplemental Table 6. Predicted effects of seven founder alleles for QTL on chromosome 4B, relative to Xi 19.

Supplemental Table 7. *TB-B1*-specific KASP marker analysis of a subset of 212 NIAB MAGIC lines.

Supplemental Table 8. Oligonucleotide sequences used in RT-qPCR assays.

Supplemental Table 9. Oligonucleotide sequences used in KASP marker assays.

Supplemental Table 10. Oligonucleotide sequences used in digital droplet PCR assays.

Supplemental Data Set 1. Paired spikelet phenotypes for modern winter wheat cultivars.

Supplemental Data Set 2. Summary of *TB-B1* allele genotypes for GEDIFLUX population.

ACKNOWLEDGMENTS

We acknowledge the Biotechnology and Biological Sciences Research Council (BBS/E/J/000C0677, BB/P016855/1, BB/M011666/1, and BB/N00518X/1), the Royal Society (UF150081), International Wheat Yield Partnership, and a CSIRO O.C.E. Fellowship for funding this research. We also acknowledge Grant Calder, Elaine Barclay, Sara Simonini, Simon Griffiths, Richard Goram, Anna Backhaus (all JIC), Matthew Moscou and Inma Hernandez-Pinzon (TSL), and Beatrice Corsi (NIAB) for technical assistance; Ben Trevaskis (CSIRO) for the *VRN1* promoter; Jacob Lage and Nicholas Bird (KWS) for access to field trials of modern wheat cultivars; and Keith Gardner (NIAB) for genetic mapping guidance. We thank the Wheat Genetic Improvement Network for access to the GEDIFLUX collection. We thank the International Wheat Genome Sequencing Consortium for prepublication access to the wheat genome RefSeq v0.4 and v1.0 that was used to identify genes located in the chromosome 4D region.

AUTHOR CONTRIBUTIONS

S.A.B., L.E.D., J.R.G., and S.M.S. designed the research. S.A.B. and L.E.D. performed phenotype and genotype analyses of wild-type and *hb* plants, modern wheat cultivars, and MAGIC lines, and conducted expression analyses. S.A.B. and J.R.G. performed crosses using the *hb* line. J.R.G. analyzed transgenic plants and performed expression analysis. S.B. performed Y2H and BiFC assays. P.Z. performed FISH experiments. J.C. and G.M. collected MAGIC phenotype data and performed QTL analysis. S.M.S., K.R., and C.C. performed initial genotype analysis and characterization of MAGIC line 0053. S.A.B., L.E.D., and J.R.G. wrote the manuscript.

Received December 19, 2017; revised January 22, 2018; accepted February 10, 2018; published February 14, 2018.

REFERENCES

Abe, M., Kobayashi, Y., Yamamoto, S., Daimon, Y., Yamaguchi, A., Ikeda, Y., Ichinoki, H., Notaguchi, M., Goto, K., and Araki, T. (2005). FD, a bZIP protein mediating signals from the floral pathway integrator FT at the shoot apex. Science **309:** 1052–1056.

Aguilar-Martínez, J.A., Poza-Carrión, C., and Cubas, P. (2007). Arabidopsis *BRANCHED1* acts as an integrator of branching signals within axillary buds. Plant Cell **19:** 458–472.

Alonso-Peral, M.M., Oliver, S.N., Casao, M.C., Greenup, A.A., and Trevaskis, B. (2011). The promoter of the cereal VERNALIZATION1 gene is sufficient for transcriptional induction by prolonged cold. PLoS One **6:** e29456.

Altschul, S.F., Gish, W., Miller, W., Myers, E.W., and Lipman, D.J. (1990). Basic local alignment search tool. J. Mol. Biol. **215:** 403–410.

Beales, J., Turner, A., Griffiths, S., Snape, J.W., and Laurie, D.A. (2007). A pseudo-response regulator is misexpressed in the photoperiod insensitive *Ppd-D1a* mutant of wheat (*Triticum aestivum* L.). Theor. Appl. Genet. **115:** 721–733.

Bedbrook, J.R., Jones, J., O'Dell, M., Thompson, R.D., and Flavell, R.B. (1980). A molecular description of telometic heterochromatin in *Secale* species. Cell **19:** 545–560.

Belda-Palazón, B., Ruiz, L., Martí, E., Tárraga, S., Tiburcio, A.F., Culiáñez, F., Farràs, R., Carrasco, P., and Ferrando, A. (2012). Aminopropyltransferases involved in polyamine biosynthesis localize preferentially in the nucleus of plant cells. PLoS One **7:** e46907.

Boden, S.A., Cavanagh, C., Cullis, B.R., Ramm, K., Greenwood, J., Jean Finnegan, E., Trevaskis, B., and Swain, S.M. (2015). *Ppd-1* is a key regulator of inflorescence architecture and paired spikelet development in wheat. Nat. Plants **1:** 14016.

Boden, S.A., Weiss, D., Ross, J.J., Davies, N.W., Trevaskis, B., Chandler, P.M., and Swain, S.M. (2014). *EARLY FLOWERING3* regulates flowering in spring barley by mediating gibberellin production and *FLOWERING LOCUS T* expression. Plant Cell **26:** 1557–1569.

Bolker, B.M., Brooks, M.E., Clark, C.J., Geange, S.W., Poulsen, J.R., Stevens, M.H.H., and White, J.-S.S. (2009). Generalized linear mixed models: a practical guide for ecology and evolution. Trends Ecol. Evol. (Amst.) **24:** 127–135.

Bommert, P., Nagasawa, N.S., and Jackson, D. (2013). Quantitative variation in maize kernel row number is controlled by the *FASCIATED EAR2* locus. Nat. Genet. **45:** 334–337.

Borrill, P., Ramirez-Gonzalez, R., and Uauy, C. (2016). expVIP: a customizable RNA-seq data analysis and visualization platform. Plant Physiol. **170:** 2172–2186.

Clavijo, B.J., et al. (2017). An improved assembly and annotation of the allohexaploid wheat genome identifies complete families of agronomic genes and provides genomic evidence for chromosomal translocations. Genome Res. **27:** 885–896.

Crop Committee Handbook (2013). Crop Committee Handbook. (Kenilworth, UK: Agriculture and Horticulture Development Board Cereals and Oilseeds).

Debernardi, J.M., Lin, H., Chuck, G., Faris, J.D., and Dubcovsky, J. (2017). microRNA172 plays a crucial role in wheat spike morphogenesis and grain threshability. Development **144:** 1966–1975.

Dobrovolskaya, O., et al. (2015). FRIZZY PANICLE drives supernumerary spikelets in bread wheat. Plant Physiol. **167:** 189–199.

Doebley, J., Stec, A., and Gustus, C. (1995). *teosinte branched1* and the origin of maize: evidence for epistasis and the evolution of dominance. Genetics **141:** 333–346.

Doebley, J., Stec, A., and Hubbard, L. (1997). The evolution of apical dominance in maize. Nature **386:** 485–488.

Egea-Cortines, M., Saedler, H., and Sommer, H. (1999). Ternary complex formation between the MADS-box proteins SQUAMOSA, DEFICIENS and GLOBOSA is involved in the control of floral architecture in *Antirrhinum majus.* EMBO J. **18:** 5370–5379.

Fischer, T., Byerlee, D., and Edmeades, G. (2014). Crop Yields and Global Food Security. (Canberra, Australia: Australian Centre of International Agricultural Research).

Gardner, K.A., Wittern, L.M., and Mackay, I.J. (2016). A highly recombined, high-density, eight-founder wheat MAGIC map reveals extensive segregation distortion and genomic locations of introgression segments. Plant Biotechnol. J. **14:** 1406–1417.

González, F.G., Miralles, D.J., and Slafer, G.A. (2011). Wheat floret survival as related to pre-anthesis spike growth. J. Exp. Bot. **62:** 4889–4901.

González-Navarro, O.E., Griffiths, S., Molero, G., Reynolds, M.P., and Slafer, G.A. (2015). Dynamics of floret development determining differences in spike fertility in an elite population of wheat. Field Crops Res. **172:** 21–31.

Greenwood, J.R., Finnegan, E.J., Watanabe, N., Trevaskis, B., and Swain, S.M. (2017). New alleles of the wheat domestication geneQreveal multiple roles in growth and reproductive development. Development **144:** 1959–1965.

Guo, Z., and Schnurbusch, T. (2015). Variation of floret fertility in hexaploid wheat revealed by tiller removal. J. Exp. Bot. **66:** 5945–5958.

Hedden, P. (2003). The genes of the Green Revolution. Trends Genet. **19:** 5–9.

Houston, K., et al. (2013). Variation in the interaction between alleles of HvAPETALA2 and microRNA172 determines the density of grains on the barley inflorescence. Proc. Natl. Acad. Sci. USA **110:** 16675–16680.

Huang, B.E., and George, A.W. (2011). R/mpMap: a computational platform for the genetic analysis of multiparent recombinant inbred lines. Bioinformatics **27:** 727–729.

Huang, B.E., George, A.W., Forrest, K.L., Kilian, A., Hayden, M.J., Morell, M.K., and Cavanagh, C.R. (2012). A multiparent advanced generation inter-cross population for genetic analysis in wheat. Plant Biotechnol. J. **10:** 826–839.

Hubbard, L., McSteen, P., Doebley, J., and Hake, S. (2002). Expression patterns and mutant phenotype of teosinte branched1 correlate with growth suppression in maize and teosinte. Genetics **162:** 1927–1935.

Ishida, Y., Tsunashima, M., Hiei, Y., and Komari, T. 2015. Wheat transformation. In *Agrobacterium* Protocols: Methods in Molecular Biology, K. Wang, ed (New York: Springer), pp. 189–198.

Jiao, Y., Wang, Y., Xue, D., Wang, J., Yan, M., Liu, G., Dong, G., Zeng, D., Lu, Z., Zhu, X., Qian, Q., and Li, J. (2010). Regulation of *OsSPL14* by *OsmiR156* defines ideal plant architecture in rice. Nat. Genet. **42:** 541–544.

Kosugi, S., and Ohashi, Y. (1997). PCF1 and PCF2 specifically bind to cis elements in the rice proliferating cell nuclear antigen gene. Plant Cell **9:** 1607–1619.

Krasileva, K.V., et al. (2017). Uncovering the hidden variation in polyploid wheat. Proc. Natl. Acad. Sci. USA **114:** E913–E921.

Kyozuka, J., Tokunaga, H., and Yoshida, A. (2014). Control of grass inflorescence form by the fine-tuning of meristem phase change. Curr. Opin. Plant Biol. **17:** 110–115.

Lemmon, Z.H., Park, S.J., Jiang, K., Van Eck, J., Schatz, M.C., and Lippman, Z.B. (2016). The evolution of inflorescence diversity in the nightshades and heterochrony during meristem maturation. Genome Res. **26:** 1676–1686.

Lewis, J.M., Mackintosh, C.A., Shin, S., Gilding, E., Kravchenko, S., Baldridge, G., Zeyen, R., and Muehlbauer, G.J. (2008). Overexpression of the maize *Teosinte Branched1* gene in wheat suppresses tiller development. Plant Cell Rep. **27:** 1217–1225.

Li, C., Lin, H., and Dubcovsky, J. (2015). Factorial combinations of protein interactions generate a multiplicity of florigen activation complexes in wheat and barley. Plant J. **84:** 70–82.

Luo, D., Carpenter, R., Vincent, C., Copsey, L., and Coen, E. (1996). Origin of floral asymmetry in *Antirrhinum.* Nature **383:** 794–799.

Mackay, I.J., Bansept-Basler, P., Barber, T., Bentley, A.R., Cockram, J., Gosman, N., Greenland, A.J., Horsnell, R., Howells, R., O'Sullivan, D.M., Rose, G.A., and Howell, P.J. (2014). An eight-parent multiparent advanced generation inter-cross population for winter-sown wheat: creation, properties, and validation. G3 (Bethesda) **4:** 1603–1610.

Meyer, R.S., and Purugganan, M.D. (2013). Evolution of crop species: genetics of domestication and diversification. Nat. Rev. Genet. **14:** 840–852.

Mieog, J.C., Howitt, C.A., and Ral, J.-P. (2013). Fast-tracking development of homozygous transgenic cereal lines using a simple and highly flexible real-time PCR assay. BMC Plant Biol. **13:** 71.

Milner, S.G., Maccaferri, M., Huang, B.E., Mantovani, P., Massi, A., Frascaroli, E., Tuberosa, R., and Salvi, S. (2016). A multiparental cross population for mapping QTL for agronomic traits in durum wheat (*Triticum turgidum* ssp. durum). Plant Biotechnol. J. **14:** 735–748.

Miralles, D., Richards, R.A., and Slafer, G.A. (2000). Duration of the stem elongation period influences the number of fertile florets in wheat and barley. Aust. J. Plant Physiol. **27:** 931–940.

Miura, K., Ikeda, M., Matsubara, A., Song, X.-J., Ito, M., Asano, K., Matsuoka, M., Kitano, H., and Ashikari, M. (2010). *OsSPL14* promotes panicle branching and higher grain productivity in rice. Nat. Genet. **42:** 545–549.

Mukai, Y., Nakahara, Y., and Yamamoto, M. (1993). Simultaneous discrimination of the three genomes in hexaploid wheat by multicolor fluorescence in situ hybridization using total genomic and highly repeated DNA probes. Genome **36:** 489–494.

Niwa, M., Daimon, Y., Kurotani, K., Higo, A., Pruneda-Paz, J.L., Breton, G., Mitsuda, N., Kay, S.A., Ohme-Takagi, M., Endo, M., and Araki, T. (2013). BRANCHED1 interacts with FLOWERING LOCUS T to repress the floral transition of the axillary meristems in *Arabidopsis.* Plant Cell **25:** 1228–1242.

Park, S.J., Jiang, K., Schatz, M.C., and Lippman, Z.B. (2012). Rate of meristem maturation determines inflorescence architecture in tomato. Proc. Natl. Acad. Sci. USA **109:** 639–644.

Park, S.J., Jiang, K., Tal, L., Yichie, Y., Gar, O., Zamir, D., Eshed, Y., and Lippman, Z.B. (2014). Optimization of crop productivity in tomato using induced mutations in the florigen pathway. Nat. Genet. **46:** 1337–1342.

Paterson, A.H., Brubaker, C.L., and Wendel, J.F. (1993). A rapid method for extraction of cotton (*Gossypium* ssp.) genomic DNA suitable for RFLP and PCR analysis. Plant Mol. Biol. Report. **11:** 122–127.

Pearce, S., et al. (2011). Molecular characterization of *Rht-1* dwarfing genes in hexaploid wheat. Plant Physiol. **157:** 1820–1831.

Poursarebani, N., et al. (2015). The genetic basis of composite spike form in barley and 'Miracle-Wheat'. Genetics **201:** 155–165.

Ramirez-Gonzalez, R.H., Uauy, C., and Caccamo, M. (2015a). PolyMarker: a fast polyploid primer design pipeline. Bioinformatics **31:** 2038–2039.

Ramirez-Gonzalez, R.H., Segovia, V., Bird, N., Fenwick, P., Holdgate, S., Berry, S., Jack, P., Caccamo, M., and Uauy, C. (2015b). RNA-Seq bulked segregant analysis enables the identification of high-resolution genetic markers for breeding in hexaploid wheat. Plant Biotechnol. J. **13:** 613–624.

Ramsay, L., et al. (2011). *INTERMEDIUM-C*, a modifier of lateral spikelet fertility in barley, is an ortholog of the maize domestication gene *TEOSINTE BRANCHED 1.* Nat. Genet. **43:** 169–172.

Rawson, H.M. (1970). Spikelet number, its control and relation to yield per ear in wheat. Aust. J. Biol. Sci. **23:** 1–15.

Rayburn, A.L., and Gill, B.S. (1986). Isolation of a D-genome specific repeated DNA sequence from *Aegilops squarrosa.* Plant Mol. Biol. Report. **4:** 102–109.

Reynolds, M., Foulkes, M.J., Slafer, G.A., Berry, P., Parry, M.A.J., Snape, J.W., and Angus, W.J. (2009). Raising yield potential in wheat. J. Exp. Bot. **60:** 1899–1918.

Richardson, T., Thistleton, J., Higgins, T.J., Howitt, C., and Ayliffe, M. (2014). Efficient *Agrobacterium* transformation of elite wheat germplasm without selection. Plant Cell Tissue Organ Cult. **119:** 647–659.

Sainsbury, F., Thuenemann, E.C., and Lomonossoff, G.P. (2009). *pEAQ*: versatile expression vectors for easy and quick transient expression of heterologous proteins in plants. Plant Biotechnol. J. **7:** 682–693.

Schindelin, J., et al. (2012). Fiji: an open-source platform for biological-image analysis. Nat. Methods **9:** 676–682.

Sharman, B.C. (1944). Branched heads in wheat and wheat hybrids. Nature **153:** 497–498.

Sharman, B.C. (1967). Interpretation of the morphology of various naturally occurring abnormalities of the inflorescence of wheat *(Triticum*). Can. J. Bot. **45:** 2073–2080.

Shaw, L.M., Turner, A.S., and Laurie, D.A. (2012). The impact of photoperiod insensitive *Ppd-1a* mutations on the photoperiod pathway across the three genomes of hexaploid wheat (*Triticum aestivum*). Plant J. **71:** 71–84.

Simons, K.J., Fellers, J.P., Trick, H.N., Zhang, Z., Tai, Y.-S., Gill, B.S., and Faris, J.D. (2006). Molecular characterization of the major wheat domestication gene *Q.* Genetics **172:** 547–555.

Slafer, G.A. (2003). Genetic basis of yield as viewed from a crop physiologist's perspective. Ann. Appl. Biol. **142:** 117–128.

Soyk, S., et al. (2017). Bypassing negative epistasis on yield in tomato imposed by a domestication gene. Cell **169:** 1142–1155.e12.

Studer, A., Zhao, Q., Ross-Ibarra, J., and Doebley, J. (2011). Identification of a functional transposon insertion in the maize domestication gene tb1. Nat. Genet. **43:** 1160–1163.

Studer, A.J., Wang, H., and Doebley, J.F. (2017). Selection during maize domestication targeted a gene network controlling plant and inflorescence architecture. Genetics **207:** 755–765.

Takeda, T., Suwa, Y., Suzuki, M., Kitano, H., Ueguchi-Tanaka, M., Ashikari, M., Matsuoka, M., and Ueguchi, C. (2003). The *OsTB1* gene negatively regulates lateral branching in rice. Plant J. **33:** 513–520.

Talbot, M.J., and White, R.G. (2013). Methanol fixation of plant tissue for scanning electron microscopy improves preservation of tissue morphology and dimensions. Plant Methods **9:** 36.

Taoka, K., et al. (2011). 14-3-3 proteins act as intracellular receptors for rice Hd3a florigen. Nature **476:** 332–335.

Tatematsu, K., Nakabayashi, K., Kamiya, Y., and Nambara, E. (2008). Transcription factor AtTCP14 regulates embryonic growth potential during seed germination in Arabidopsis thaliana. Plant J. **53:** 42–52.

Tenesa, A., and Haley, C.S. (2013). The heritability of human disease: estimation, uses and abuses. Nat. Rev. Genet. **14:** 139–149.

The UniProt Consortium (2017). UniProt: the universal protein knowledgebase. Nucleic Acids Res. **45:** D158–D169.

Wang, L., Sun, S., Jin, J., Fu, D., Yang, X., Weng, X., Xu, C., Li, X., Xiao, J., and Zhang, Q. (2015). Coordinated regulation of vegetative and reproductive branching in rice. Proc. Natl. Acad. Sci. USA **112:** 15504–15509.

Wang, S., et al.; International Wheat Genome Sequencing Consortium (2014). Characterization of polyploid wheat genomic diversity using a high-density 90,000 single nucleotide polymorphism array. Plant Biotechnol. J. **12:** 787–796.

Watson, A., et al. (2018). Speed breeding is a powerful tool to accelerate crop research and breeding. Nat. Plants **4:** 23–29.

Wigge, P.A., Kim, M.C., Jaeger, K.E., Busch, W., Schmid, M., Lohmann, J.U., and Weigel, D. (2005). Integration of spatial and temporal information during floral induction in Arabidopsis. Science **309:** 1056–1059.

Wu, T.D., and Watanabe, C.K. (2005). GMAP: a genomic mapping and alignment program for mRNA and EST sequences. Bioinformatics **21:** 1859–1875.

Yan, L., Loukoianov, A., Tranquilli, G., Helguera, M., Fahima, T., and Dubcovsky, J. (2003). Positional cloning of the wheat vernalization gene *VRN1.* Proc. Natl. Acad. Sci. USA **100:** 6263–6268.

Yano, K., et al. (2015). Isolation of a novel lodging resistance QTL gene involved in strigolactone signaling and its pyramiding with a QTL gene involved in another mechanism. Mol. Plant **8:** 303–314.

Yoshida, A., et al. (2013). *TAWAWA1*, a regulator of rice inflorescence architecture, functions through the suppression of meristem phase transition. Proc. Natl. Acad. Sci. USA **110:** 767–772.

Zhang, D., and Yuan, Z. (2014). Molecular control of grass inflorescence development. Annu. Rev. Plant Biol. **65:** 553–578.

Zhang, P., Li, W., Fellers, J., Friebe, B., and Gill, B.S. (2004). BAC-FISH in wheat identifies chromosome landmarks consisting of different types of transposable elements. Chromosoma **112:** 288–299.

Zhu, Z., Tan, L., Fu, Y., Liu, F., Cai, H., Xie, D., Wu, F., Wu, J., Matsumoto, T., and Sun, C. (2013). Genetic control of inflorescence architecture during rice domestication. Nat. Commun. **4:** 2200.